First FLASH Investigations Using a 35 MeV Electron Beam From the Duke/TUNL High Intensity Gamma-ray Source

by

Markus Theodor Sprenger

Graduate Program in Medical Physics
Duke University

Date:_____

Approved:

_____
Mark Oldham, Supervisor

_____
Scott Floyd

_____
Ying Wu

Thesis submitted in partial fulfillment of the requirements for the degree of Master of Science in the Graduate Program in Medical Physics in the Graduate School of Duke University

2023

ABSTRACT

First FLASH Investigations Using a 35 MeV Electron Beam From the Duke/TUNL High Intensity Gamma-ray Source

by

Markus Theodor Sprenger

Graduate Program in Medical Physics
Duke University

Date:_____

Approved:

_____
Mark Oldham, Supervisor

_____
Scott Floyd

_____
Ying Wu

An abstract of a thesis submitted in partial fulfillment of the requirements for the degree of Master of Science in the Graduate Program in Medical Physics in the Graduate School of Duke University

2023

Abstract

Purpose: Current cancer treatment methods makes use of radiation, usually in combination with other therapeutic drugs. A common method of delivering radiation is through external radiation beam delivery, which can be done using a medical linear accelerator in a photon and/or electron mode in the energy range of 6-20 MeV with a mean and instantaneous dose rate of 0.17 Gy/s and 200 Gy/s, respectively. Recent investigations into external beam radiation dose-rate dependencies of normal tissue health have rekindled a growing interest in FLASH radiotherapy, occurring at mean dose rates greater than 40 Gy/s and instantaneous dose rates greater than 10^5 Gy/s. FLASH radiotherapy is denoted by its ability to spare normal tissue, but maintain equal tumor control compared to conventional dose rates used in the clinic. Technological advancements have made higher dose rates more feasible to achieve in a clinical setting making FLASH radiotherapy a more accessible option for cancer treatment compared to previous decades. The underlying biological mechanisms of the normal tissue sparing in FLASH radiotherapy, described as the FLASH effect, are still unknown and developing an in vitro model to study it has proven difficult. This work aims to combine two unique technologies, an *ex vivo* organotypic rat brain slice model which models the micro-environment in a controlled setting and a linear accelerator capable of delivering variable FLASH dose rate pulses to design experiments which will facility the study of

the FLASH effect. These two technologies are used to explore differences in the cyto-toxic response of 4T1 cancer cells to FLASH and conventional irradiation dose rates.

Methods: The experiments utilize a 35 MeV electron beam provided by Triangle Universities Nuclear Laboratory's (TUNL) High Intensity Gamma-ray Source linac (HIGS) on Duke University's west campus. The beam can supply electron pulses with variable charge and a temporal width of 1.2 μs or 100 ns. Dosimetry was performed with Gafchromic EBT3 and EBT-XD film to determine the dose and dose rates of each pulse to within 4%. Experiments were performed over 6 sessions to establish the use and effectiveness of combining the HIGS linac and biological rat brain model. A 2D translational stage and targeting quality assurance procedures were developed to ensure accurate targeting for each of 8 wells containing an organotypic rat brain slice in a 12 well plate. Each rat brain slice was shot with a yellow fluorescent protein marker and seeded with 4T1 cancer cells tagged with mCherry and firefly luciferase. An imaging analysis workflow was developed to effectively segment mCherry signal and determine the 4T1 proliferation four to five days after irradiation. The mCherry analysis is compared to an independent final firefly luciferase assay readout. Each experiment using the HIGS was followed by a conventional irradiation, using a Varian 21EX Clinac, as a control group. Monte Carlo modeling using TOPAS was created to simulate the HIGS linac dose profiles to explore the major contributions to dose and dose shape.

Results: The HIGS linac can currently provide a mean dose rate of up to 100 Gy/s and instantaneous dose rates up to 100 MGy/s. The repeatability of the pulse dose was found to be within 4-5% of the average dose for a given experiment with a field size of approximately 1.3x2 cm^2. Pulse targeting and dose superposition was confirmed to be repeatable with the field size changing by 0.4 ± 0.2 mm when using multiple pulses. Well targeting quality assurance procedures of the translational stage allowed for consistent targeting of the pulse to each well as recorded in film measurements. The mCherry workflow effectively filtered out any yellow fluorescent protein bleed through into the mCherry signal and the mCherry analysis reflects the end readout of the independent firefly luciferase assay. The HIGS linac FLASH irradiation was found to reduce cell growth in the 0-7 Gy range, but the conventional irradiation effects on the 4T1 cell growth is not clear on this same dose range. A gamma analysis performed between the simulated HIGS beam using TOPAS and gafchromic film measured doses demonstrate a passing rate of 99.4% when using the criteria of 2%/2mm and a dose threshold of 10%.

Conclusions: FLASH capable dose rates can be supplied by the HIGS linac and are amongst the highest instantaneous dose rates currently available. The HIGS linac and organotypic rat brain model can be combined to irradiate and measure FLASH radiation effects on 4T1 cancer cell growth below 10 Gy. Future work can be done to overcome saturation effects above 10 Gy and increase the sensitivity and strength of the mCherry

and the firefly luciferase analysis. Qualitative data supports the observation of the FLASH effect in the rat brain model. The mCherry and firefly luciferase analysis agreement demonstrates the capabilities of the organotypic model to measure radiation effects to cancer cells in the 1-10 Gy range. Future work will be to quantitively measure the neuron health of the brain slices and DNA damage differences between FLASH and conventional irradiation. Monte Carlo simulations of the HIGS beam will be a useful tool for investigating beam and dose features in addition to paving the way for small animal experiments.

Contents

List of Tables

List of Figures

Acknowledgements

I would like to acknowledge Anna Lynnette Price, Wei Li, Denise Dunn and Stepan Mikhailov for their significant contributions to this collaboration. Thank you to the senior faculty of this endeavor who also served on my committee: Mark Oldham, Scott Floyd, and Ying Wu.

1. Introduction

This thesis documents the first investigations of the potential for Triangle Universities Nuclear Laboratory's High Intensity Gamma Ray Source (HIGS) as a unique technology with capabilities to comprehensively explore FLASH radiotherapy dose rates and its underlying mechanisms of action. The second aim of this work is to explore combining the HIGS linac FLASH dose rates with a novel organotypic live-tissue rat brain slice model for the study of ultra-high dose rates effects on normal tissue and cancer cells. Attention was focused to the cyto-toxic response of the cancer cells to radiation in the organotypic model. The following sections will introduce the current state of FLASH radiotherapy and background on important technology, software and terminology used in this work.

1.1 FLASH Radiotherapy

The coining of the term FLASH radiotherapy (FLASH-RT) was first done by Marie-Catherine Vozenin who rediscovered the normal tissue sparing effect of radiation delivered with mean dose rates >40 Gy/s [1]. FLASH-RT performed on cats, mini-pigs, mice, and other animals have demonstrated how normal tissue can tolerate high dose rate radiation more effectively than current conventional dose rates [1-4]. More importantly, the tumor control rate is reported to be unchanged with the increase in dose rate[4]. The adopted mean dose rate threshold has become 40 Gy/s for FLASH-RT; however, the true mechanisms behind the FLASH effect and the importance of mean

dose rate (MDR) to instantaneous dose rate (IDR) for achieving the FLASH effect remain unknown. It is also not clear if all cancer cells are controlled equally between FLASH and conventional dose rates as some studies have demonstrated the normal tissue sparing FLASH effect in prostate cancer cells [5]. Understanding the FLASH mechanism is becoming critically important with the recent completion of the first FLASH-RT clinical trial FAST-01 which treated bone metastases with proton FLASH-RT [6]. Some hypotheses for the normal tissue sparing effect of FLASH-RT include:

1. Transient Hypoxia: Sudden oxygen consumption in the normal tissue by incoming FLASH dose rate radiation creates a temporary hypoxic environment which the blood is not able to quickly resupply. This transient hypoxia prevents the fixation of further DNA damage [7, 8].
2. Immune System Sparing: Due to the fast treatment time there is little to no blood flow through the radiation beam field and circulating lymphocytes in the blood are spared [7].
3. Stem Cell Hypoxia: stem-cell niches are hypoxic environments allowing for the radioprotection of stem cells due to the increased oxygen consumption of FLASH dose rates [9, 10]. Like hypothesis 1, but is limited to the stem cell niches, rather than all normal tissue.

4. DNA damage differences: This hypothesis proposes that DNA damage induced by FLASH-RT is inherently different than that of conventional radiotherapy methods.

This direction of this work is to demonstrate the capabilities of the HIGS linac to probe different mean and instantaneous dose rates to observe MRD or IDR dose rate dependencies of normal tissue sparing and cancer cell growth. The ability to vary the HIGS linac MDR and IDR will allow for future work to inquire about the DNA damage occurring in the normal tissue and cancer cells of the rat brain slice to understand the underlying mechanisms of FLASH-RT.

Some primary difficulties with studying the FLASH effect are replicating it in an in vitro setting. Not only do the majority of the above hypothesis rely on blood flow, thus limiting the viable in vitro models, not much work has been published on observing the FLASH effect in an in vitro setting. We anticipate the organotypic model to model the in vivo environment more closely allowing for observation of the FLASH effect. This work will focus on an organotypic model in combination with the HIGS linac to measure the proliferation of 4T1 mouse breast cancer cells in response to variable doses as a comparison to study cancer cell response and gauge possible concern of cancer cell sparing when using FLASH dose rates [4, 5].

1.2 HIGS: High Intensity Gamma Ray Source Linear Accelerator

To understand the need for a resource like the High Intensity Gamma-ray Source (HIGS), we will first look at linear accelerator technology currently used in radiation therapy. There is a large variability of models across multiple vendors, but the general magnitude of the mean dose rate, 1000 MU/min or 10 Gy/min, is similar across them all. This is equivalent to 0.17 Gy/s. A typical pulse width and repetition time for a Varian linac is 5 μs and 180 Hz or 5 ms respectively. This leads to an instantaneous dose rate of 185 Gy/s. When aggressively restraining the x-ray target and overriding numerous safety interlocks, one would expect the dose rate to then increase by approximately a factor of 1000. This increases the MDR to 170 Gy/s and IDR at 1.85×10^5 Gy/s. As mentioned previously, we wish to achieve an IDR greater than 10^5 Gy/s and a MDR greater than 40 Gy/s. Comparing these theoretical calculations to experimental work: a group from Dartmouth performed modifications to a Varian Clinac 2100 C/D with a repetition rate of 360 Hz. By restraining the x-ray target along with other modifications frowned upon by Varian , they achieved mean dose rates of approximately 290 Gy/s using a 10 MeV electron beam [11, 12]. It is not reasonably safe to attain FLASH dose rates with current medical linear accelerator technology in Duke Radiation Oncology; therefore, a need for a new piece of technology, capable of achieving FLASH dose rates without risky alterations at almost clinical energies, was needed for the exploration of the FLASH effect.

A key tool used in this thesis is the Triangle Universities Nuclear Laboratory's (TUNL) HIGS linac as a 35 MeV electron source. The linac is part of a larger facility, seen in figure 1, feeding a 0.18 to 1.2 GeV booster which then transfers the electrons to a storage ring for use in the production of a free electron laser and a final γ-ray beam. The HIGS facility is capable of accelerating electrons up to 1.2 GeV and producing a free electron laser and photons up to 120 MV. It is a world leading resource in fields of nuclear physics, biology, and material science boasting the highest-flux Compton gamma-ray source in the world [13].

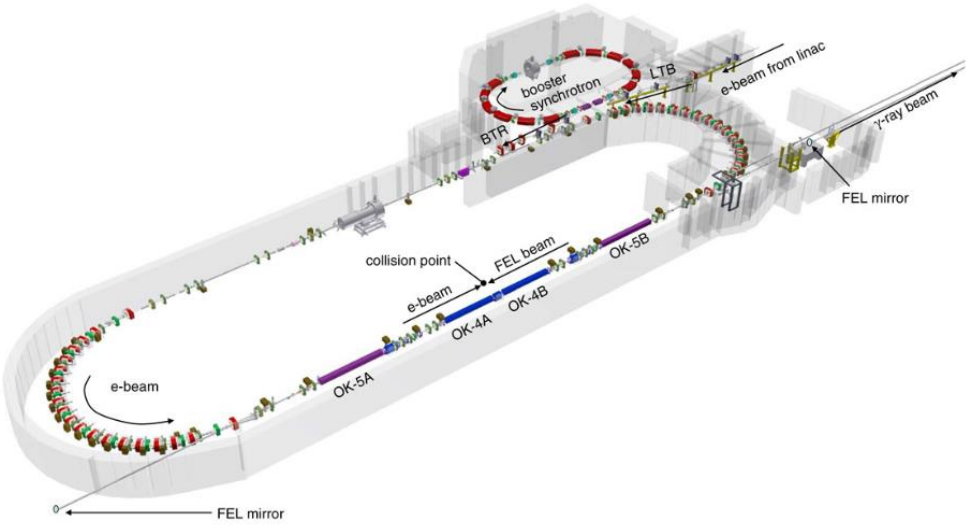

Figure 1: Drawing of the High Intensity Gamma-ray Source reprinted from Weller et al. [13, 14]. The linac, booster, storage ring, and key components are shown.

The electron beam supplied by HIGS can currently be extracted at 35 and 180 MeV. The major components of the HIGS facility relevant to this thesis are as follows: The pulse begins at the electron gun, steered through a chopper, and passes through an

energy selecting magnet. The electrons then enter the linear accelerator's traveling wave accelerating cell, operating in the S-band. At the end of the cell a dipole extracts the electron beam at 9 degrees from the beam line with an energy of approximately 35 MeV and targets an aluminum beam dump at 18.4 cm away.

Seen in figure 2, the use of nuclear and high energy physics facilities is common for the use in FLASH experiments. Outside of the NLCTA and ELBE, most electron FLASH dose rate machines struggle to exceed 10 MGy/s IDR. Electron FLASH is also seen to cover high MDR and IDR ranges making electron FLASH an ideal candidate for exploration of MDR and IDR effects in FLASH-RT. The variety of electron FLASH devices range a broad spectrum of energies from a few MeV to several hundred MeV at the CLEAR user facility at CERN [15]. In chapter 2, the HIGS linac capabilities compared to other electron machines.

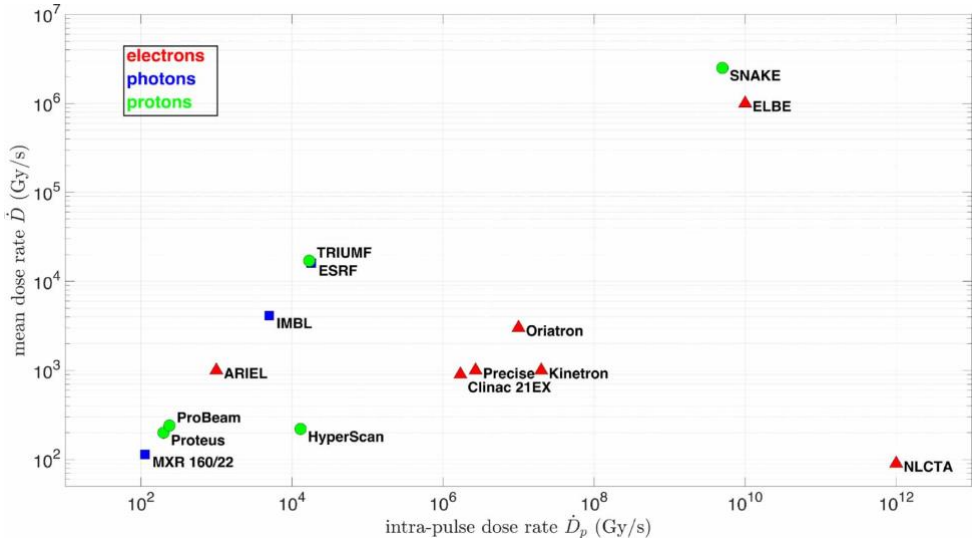

Figure 2: Comparison of MDR and IDR for current FLASH machines. Figure is reprinted from Esplen et al. [16]

1.3 Challenges of FLASH Dosimetry

Dosimetry in a FLASH dose rate environment is currently under investigation and few dose rate independent tools are available. Among these are thermoluminescent dosimeters, gafchromic film and alanine pallets with a minimum error of 3% of the true dose [4]. We elected to use gafchromic film, Ashland EBT3 and EBT-XD, for FLASH dosimetry as it is reported to be dose rate independent [17] and we found to be relatively energy independent in the 20-35 MeV electron energy range, as explained in section 2.2.2.3. The film also allows for resolving a 2D dose map of the HIGS linac.

EBT3 film has a dynamic dose range of 0.1 to 20 Gy [18] and EBT-XD film has a dynamic dose range of 0.1 to 60 Gy [19]. However, EBT3 and EBT-XD film optimal dose range are below 10 Gy and 40 Gy respectively [18, 19]. Due to their differing sensitivity ranges, EBT 3 film is preferred for low dose experiments or plate targeting QA and EBT-XD is preferred when the dose exceeds 10 Gy due to its minimized artifacts [20]. When beginning this work, film analysis procedures were revised, and new procedures developed to remove artifacts. Current lab techniques improved film dosimetry accuracy to within 4% percent. The dose to pulse charge was also checked to ensure that film calibration with 20 MeV electrons was still valid when using 35 MeV electrons.

Film calibration was modeled using a third-degree polynomial to relate optical density to dose. Literature favors a logarithmic fit as it is considered to have a stronger basis in physical reality to film response [18, 19, 21]; however, it is noted that a third-

degree polynomial fit is also acceptable but should not be used to extrapolate to doses outside the fitted region [18, 19]. Our own calibration curves struggled to fit a logarithmic function but found a 3rd degree polynomial function provides an exceptional fit as shown in 2.1.2 Results of Improved Film Dosimetry and Calibration.

1.4 TOPAS: Tool for Particle Simulation Monte Carlo Software

Simulations of the HIGS electron beam were performed using the TOol for PArticle Simulation (TOPAS) [22, 23]. This is a Monte Carlo simulation software which is wrapped around GEANT4, see figure 3 for outline. Not only has TOPAS become largely accepted in the community, [22, 23] it has been used in our previous work [24]. TOPAS is original intended for proton therapy simulations but can be equally used for other purposes such as brachytherapy and electron therapy. It can also be extended with TOPAS n' bio for modeling of DNA damage by radiation [10]. Simulations performed with TOPAS are comprised of a hierarchy of parameter files which together create an world and environment in which particles are simulated with the desired irradiation parameters and dose can be scored to a chosen target volume. We will use TOPAS to simulate a 35 MeV electron beam and model the HIGS linac electron source starting at the dipole magnet.

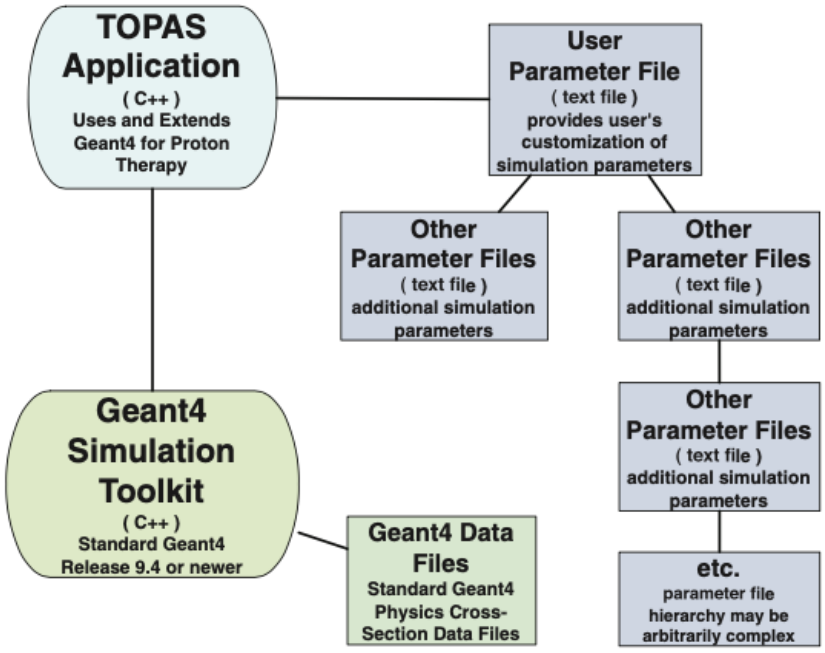

Figure 3: Flow chart of the TOPAS application utilizing a hierarchy of parameter files in relation to the GEANT4 toolkit. Reprinted from J. Perl et al. [23]

1.5 Organotypic Rat Brain Slice as Ex Vivo Model

An organotypic model comprised of a rat brain slice seeded with 4T1 cancer cells was used in this experiment. The rat brain was sliced at either 250 or 350 μm using a vibratome, dependent on the desired length of data analysis out to day 4 or 5. The preparation of the rat brain slice is widely reported in other papers [25-27]. The rat brain is placed onto a layer of nutrient rich agarose in a 12-well plate in row A and C, see figure 4. Yellow Florescent Protein (YFP) gene transfer was performed using biolistic transfection using gold nano particle bullets coated with DNA shot at the brain slices with a gene gun [28].

Figure 4: 12-well plate with rat brain slices in row A and C. This well configuration was used in all experiments.

The cell line of choice for our investigation of cancer cell response to FLASH radiation is an *in vitro* cultured, 4T1 murine mammary cancer cell line. It is tagged with mCherry and firefly luciferase (fFluc) allowing for fluorescent imaging up to 5 days following irradiation using a Zeiss Lumar V12 stereoscope and followed by an independent final fFluc readout. Comparison of the two Assays allows for verification of mCherry analysis, and proper segmentation of 4T1 cells. Much effort was performed by a previous Master's student in the Oldham lab to build a pipeline [29, 30] in CellProfiler [31] for mCherry fluorescent signal segmentation. This work aims to develop procedures

to further improve mCherry signal measurements and to filter out YFP bleed through into the mCherry images. It also looks to determine the effectiveness of FLASH irradiation to cease cancer cell growth compared to conventional irradiation.

1.6 Experiment Naming Convention

A total of 6 experiments were performed using the HIGS linac. A typical name for an experiment would be "HIGS 5b." Here HIGS or CONV refers to what machine the irradiation was performed on. HIGS refers to the High Intensity Gamma-ray Source linac whereas CONV refers to the Varian 21EX Clinac used for control conventional irradiation experiments. The following Arabic numeral enumerates the experiment number and groups together a conventional irradiation with its respective FLASH irradiation on the HIGS linac. This means that HIGS 3 and CONV 3 are the FLASH and conventional irradiation counterparts of the third experiment. It should be noted that HIGS 1 and 2 do not have an associated CONV experiment.

The final lowercase letter refers to the day or iteration of the experiment with the same experiment parameters. HIGS 5a and HIGS 5b are performed with the same HIGS linac settings and part of the same experiment but occur on two separate dates. If the final letter is omitted than all days of the experiment are implied.

HIGS 1 and 2 are for dosimetry purposes only and provide data to characterize the HIGS electron beam to establish proper well targeting and irradiation techniques. HIGS 3 and 4 established challenges with possible solutions when using the organotypic

model and CONV 3a-d was used to solve contamination issues causing many of the wells to be unusable. HIGS 6a is included in this thesis as it is the first experiment in which a mean dose rate of greater than 40 Gy/s was achieved. HIGS 5 is the combination of HIGS 1-4 and is a culmination of techniques, methods, and solutions to effectively use the organotypic model in conjunction with the HIGS linac.

1.7 Scope of Work

This work pioneers a new research direction at Duke involving a collaboration between Radiation Oncology, Medical Physics and Physics. There was no previous work associated with FLASH radiotherapy at Duke and is a new frontier which was undertaken by experienced faculty. This thesis is written to reflect the initial efforts to designing an experimental model using existing unique tools provided by each group in the collaboration. This research does make use of, and extend, cell counting algorithms developed in earlier work [29, 30].

The format of the thesis was designed to have an extensive introduction to describe the unique materials and facilities used and give the reader an overview of the complexity involved with the progress of our investigations. The following chapter is preparatory work performed before the designing of an experiment to test the organotypic model in combination with the HIGS linac. A final experiment, HIGS 5, is performed and described in detail in chapter 3 as the culmination of all preparatory efforts and the current ability of the organotypic brain slice model to study FLASH-RT.

It is followed by a chapter on Monte Carlo simulation of the HIGS linac as this tool will ultimately allow for small animal experiments and the simulation of various dose profiles and distributions. The thesis then ends with some concluding remarks on the progress and future directions of FLASH-RT research at Duke University.

2. Preparatory Experimental Work to Enable the HIGS 5 Experiment

2.1 Improved Film Dosimetry and Calibration

Lab film procedures created previously for spatially fractionated grid therapy dosimetry [32] were adopted. Scanning of EBT3 or EBT-XD film at 400 dpi was done on an EPSON 11000XL scanner. Film handling, scanning and analysis procedures followed methods on the before mentioned spatially fractionated grid therapy [32], but was further improved due to some noticeable flaws in the dosimetry data. Prior film dosimetry procedures lacked a specification of the original film orientation and did not account for film being placed at different lateral positions or distance from the scanning direction, all of which can affect the response. Film dosimetry, for spatially fractionated grid therapy, was also in the optimal dose range of EBT3 film and would not be heavily affected by scanner position; therefore, a correction was not mandatory. When beginning FLASH film dosimetry in HIGS 1, omitting film orientation and positional dependence corrections produced confounding results. As an example, the top calibration curve in figure 6 demonstrates two instances where a higher delivered dose to the EBT3 film resulted in a lower optical density.

Through testing it was discovered that the orientation of the film was important to film response and two pre-scans to ensure the proper orientation of the film on the scanner were implemented. Between pre-scan one and pre-scan two the film was rotated by 90 degrees. Both pre-scan images were imported into ImageJ and the red color

channel was selected. An average pixel value of an arbitrary sized ROI was taken for a film on both scans. The orientation is expected to affect the signal intensity by 3-7% of the average value in the ROI. It is then recorded which film orientation is the lower, or darker, value and becomes the selected orientation for film dosimetry. Which chosen orientation, light or dark, does not affect film dosimetry, but a consistency of a chosen orientation is required.

A second, more mathematically intensive, correction was made to the procedure and required the use of MATLAB to modify images. Film position relative to scanning direction is also important and is named the lateral response artifact or LRA [33]. As LRA is dependent on the scanner and the film itself, for each DPI setting or film type, a new correction code for LRA need to be made. Correction for LRA is noted in the following section.

2.1.1 Implementation of Lateral Response Artifact Correction

LRA is affected by two factors: the lateral position of the film on the scanner, see figure 5 below, and the amount of film exposure. When doses are above the optimal dose range of the film, LRA becomes more apparent and a contributing factor to error in dosimetry. The doses or radiation we wish to deliver for FLASH irradiations generally tests the film dose limits and we begin to see a larger contribution of the LRA. This artifact occurs due to the film acting as a polarized filter when the scanner light passes through it. As the lateral position of the film changes in relation to the scanning

direction, the scanner emitted light's angle of incidence changes. This causes less light to pass through as the film is moved off the central axis. The properties of this phenomena are inherent to the scanner, film, and scanning resolution. This means each scanner, film and resolution choice needs its own correction [20, 33, 34]. The general procedure followed is outlined in a paper by Lewis and Chan [34]. We followed the procedures by Lewis and Chan with the addition of a few more films to ensure rigor.

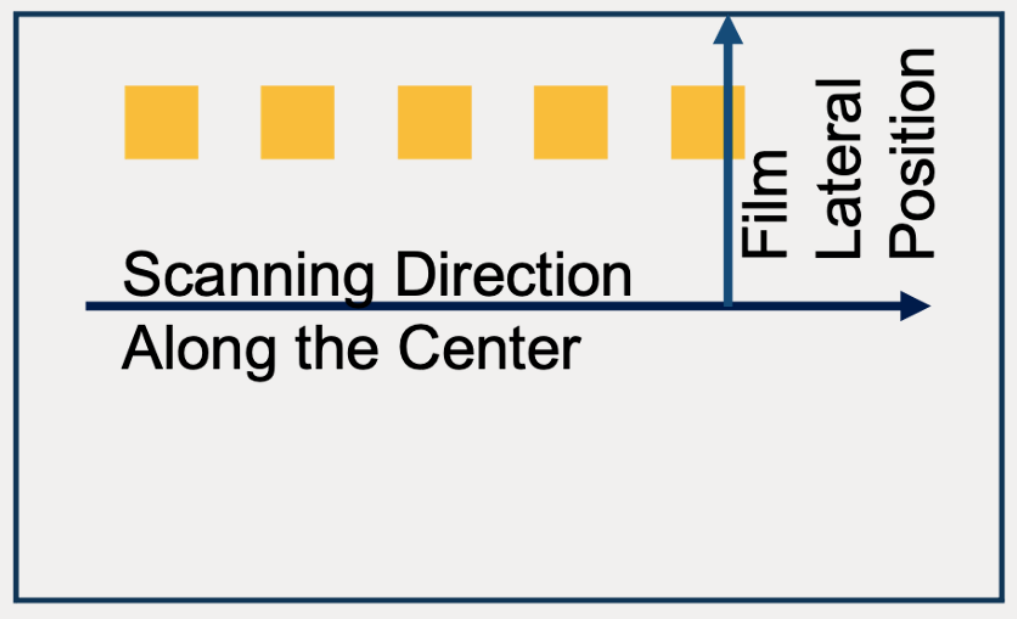

Figure 5: Depiction of scanner. Yellow squares resemble film. As the film moves off the central scanning direction their measured values change.

Seven films, irradiated with different known doses D, were placed and scanned with 400 DPI at 5 different lateral locations, L, on the scanner. The third position was located at the center of the scanner and the other positions were symmetrical (above and below) from the central axis. The red color channel was selected in ImageJ, as this is the primary color channel to perform film analysis. A 100x100 pixel region of interest was

selected at the top and bottom of each film for each position and their averages intensities were recorded. The center position film response, C, only had one ROI taken as the correction is related to response at the scanner center. In total this results in 9 positions at which coefficients were calculated. Following the first order corrections presented in Lewis and Chan and simplified for only the red color channel:

$$\text{Response}(C, D) = A_L + B_L \times \text{Response}(L, D) \qquad (2.1)$$

We fit each position to determine coefficients A_L and B_L for equation 2.1 and related the response at each position, L, to the center response of the scanner. Coefficients for pixels not directly measured are calculated by linear interpolation between the neighboring positions. For positions outside the maximum fitting range, extrapolation was used to find the coefficients. The fitted coefficients are written into a MATLAB code to apply the first order linear correction to the red color channel of each scan. After LRA corrections, images are imported into ImageJ or a separate MATLAB script for final film dosimetry measurements.

2.1.2 Results of Improved Film Dosimetry and Calibration

Three calibration curves were made using the revised techniques. One for EBT3 film in the dose range of 0-20 Gy, another for EBT-XD film in the range of 0-26 Gy and lastly a third calibration curve was made for EBT-XD film in the dose range of 0-45 Gy. Film dosimetry in FLASH irradiations were performed utilizing the improved procedures.

Figure 6 demonstrates the original EBT3 calibration curve in comparison with the calibration curve after corrections are applied. Optical density (OD) is on the x-axis of the plot and the known dose is on the y-axis. The axis was chosen to relate a known OD to an unknown dose. Error of film measurements decreases from as high as 20% to less than 5% over all film dosimetry. When film orientation or LRA corrections are omitted, film optical density is imprecise, and film irradiated with 6 Gy can be measured with a lower OD than film irradiated with 5 Gy. The R^2 for the uncorrected film calibration curve is not terrible, with a value of 0.9913; however, upon visual inspection of the upper plot from figure 6, none of the data points above 2 Gy sit well on the calibration curve. In contrast, when corrections are applied in the lower plot, the R^2 of the third-degree polynomial fit increases to a value of 0.9998. Furthermore, two films irradiated with 10 Gy are practically indistinguishable at the current axis dimensions. Error for the calibration curves falls to within 2% and even 1% in certain regions. Utilizing the improved film dosimetry procedures, dose can be measured in HIGS irradiations with approximately 4% error.

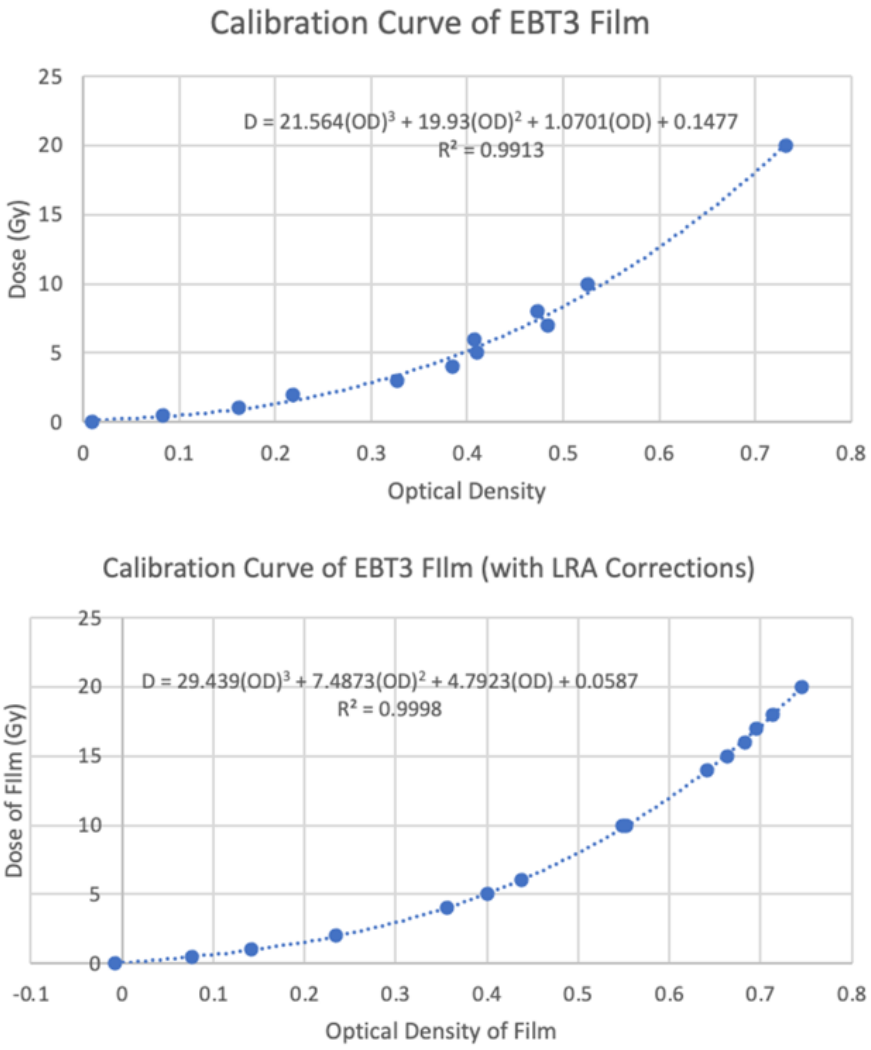

Figure 6: Top: Comparison of EBT3 calibration curve without any orientation or LRA corrections. Bottom: the calibration curve when LRA corrections are applied.

2.1.3 Testing of the Improved Calibration Curves

Improved film calibration methods were tested in CONV 3 by placing film on top of plates during irradiation. Plates were placed on 9 cm solid water allowing for the machine data tables to be used to calculate the MU needed for the delivery of prescribed

dose. The conventional irradiation set up can be seen later, in figure 19. Film was scanned and corrected for orientation and LRA in MATLAB.

The transmission (T), optical density (OD), calculated dose and error from prescribed or intended dose can be seen in table 1 seen below. Intended dose is reported as the prescribed dose in Gy and the ratio of prescribed dose to measured dose. Error reported is due to noise in the ROI across the film being propagated through the optical density calculations. 3 of the films are within 3%. The dose measured by film is accurate to within 4% when using a clinical linac and matches observations of the HIGS experiments in which the recorded dose to a well was within 4% of the average across all 4 wells. We are confident in the new film technique to be reporting the true dose to each well in our FLASH irradiations.

Table 1: EBT3 film measurements using improved film calibration and analysis methods. The ratio of Intended dose to dose is also provided.

Film	T	OD	Dose	Error	Intended Dose (%)	Intended Dose (Gy)
A	0.33747409	0.47175956	7.08	0.14	0.9967	7.1
B	0.22070295	0.65619186	14.75	0.29	1.0275	14.35
C	0.22608141	0.64573515	14.20	0.28	0.9897	14.35
D	0.34317819	0.46448032	6.85	0.14	0.9648	7.1

2.2 Determining Key HIGS-FLASH Characteristics

At the start of the HIGS 1 experiment, little was known about the pulse supplied by the HIGS linac other than an image taken with a CCD camera imaging scintillation light of the 35 MeV electron pulse passing through a paper sheet placed on the exit window, shown in figure 7. Due to the low frame rate in comparison to the pulse length

it is difficult to photograph one frame of the whole pulse, leading to the superposition of two frames. With some general information about the pulse like pulse charge, temporal width, and an estimate field size of 1.5 x 0.3 cm^2 from figure 7, a preliminary estimate of the dose per pulse was made using TOPAS Monte Carlo simulations. A 1x2 cm^2 rectangular field with 10^6 monoenergetic 35 MeV electrons with no divergence were simulated and dose was measured at 1 cm depth in a water cube with length of 5 cm. The simulated dose was scaled accounting for experimental pulse charge and field size leading to a final estimate of approximately 4 Gy per pulse. The Dose, Dose profile, pulse superposition, targeting capabilities and dose rate of the pulses delivered by the HIGS linac were unknown and characterized using EBT3 and EBT-XD film dosimetry in the following sections.

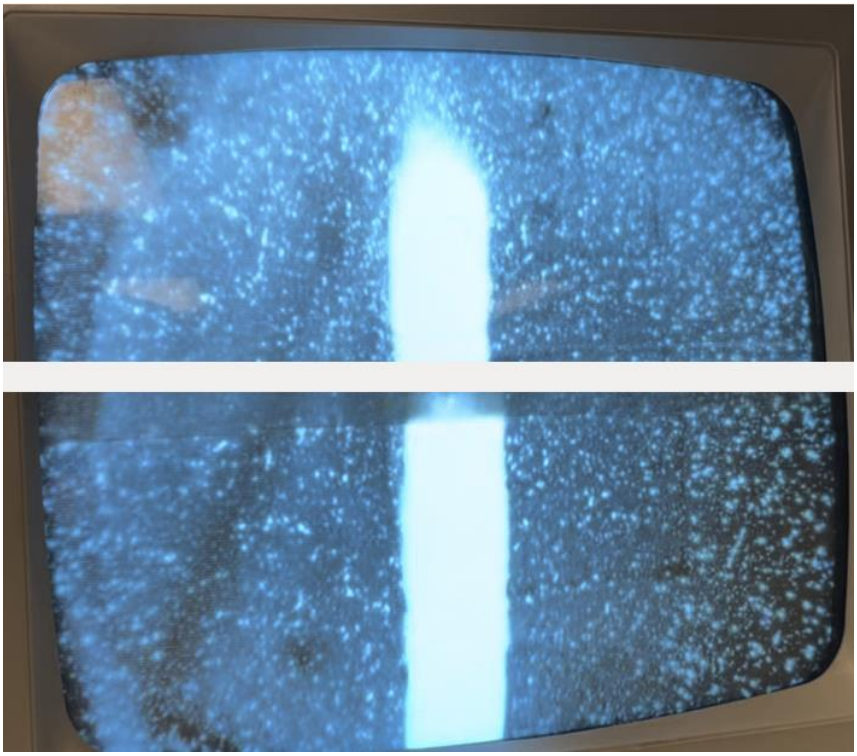

Figure 7: Initial image of HIGS pulse stitched together from two images due to the low frame rate comparatively to the short pulse length.

2.2.1 Methods of HIGS Characterization

Film dosimetry on the beam dump was used to determine an electron pulse peak dose, and dose distribution. The aluminum beam dump, also used as a Faraday cup, had a voltage read out in an oscilloscope allowing for a measurement proportional to the pulse charge. A current transformer, positioned before the 9-degree dipole magnet, allowed for measuring the pulses temporal width when pulse length was greater than 1 μs. The beam dump surface was chosen as a point of reference as it and the exit window are a fixed 18.4 cm apart, as seen in figure 8. All other components of the experiment are movable and changes in exit window to film distance would be expected. Using a fixed

distance, film dosimetry is then done at a consistent 18.4 cm away from the exit window on an experiment-to-experiment basis. For simplicity we will also call the distance from exit window to film the source to surface distance or SSD.

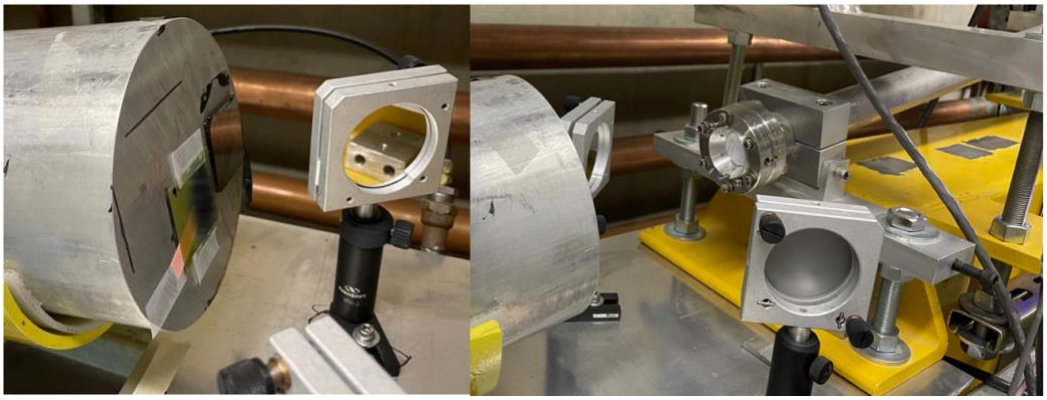

Figure 8: Left: film taped on beam dump over marked pulse location. Right: Exit window of beam line which delivers the 35 MeV electron pulse.

Film was scanned, paying attention to orientation, and corrected for LRA as before mentioned. The artifact corrected image was then imported into ImageJ where peak dose measurements were made with a 10x10 pixel ROI. Scanner images were cropped in ImageJ and imported into MATLAB for further analysis of line profiles and dose maps of the HIGS pulse.

One consideration with this setup is the aluminum beam dump providing substantial backscatter. In chapter 4 a Monte Carlo simulation of the HIGS linac is discussed with which the back scatter of the aluminum beam dump can be simulated. Monte Carlo simulations analyzing the backscatter contribution of the beam dump have found it to contribute 3.3 ± 0.3% of the dose in the primary field region.

A translational stage, built by Wei Li, minimized time between irradiations by allowing remote movement of the 12-well plate, used to house the rat brain model, from the control room. As the HIGS is a multi-user research facility and constantly undergoing alterations, well targeting needed to be checked on site before every experiment. A technique was developed, seen in figure 11 in the targeting sub-section, to allow for the visual inspection of the dose. Film was attached to the back of a dummy plate and placed in the translational stage holder. The four corner wells and two central wells of the plate were irradiated, and film was visually inspected to determine the quality of targeting. The translational stage used in HIGS4 was moving in the same coordinate system as the beam. Row A of a plate was irradiated with 1 pulse and row b was irradiated with 2 pulses. This allowed for film dosimetry of dose to well and an observation of pulse superposition and targeting by analyzing the 1 and 3 pulse Full Width Half Maximum (FWHM).

Lastly, in HIGS 2 the voltage of each pulse was recorded and plotted in comparison with film measured peak dose. A linear relation was then found between the Faraday cup voltage and peak dose. The observation of a linear relation between pulse charge and dose would support the energy independence of EBT3 and EBTXD film in the 20-35 MeV electron energy range.

2.2.2 HIGS Characterization

2.2.2.1 Pulse Dose, Dose rate, Profile and Shape

Peak dose was tunable between 0.45 to 6 Gy at the beam dump. For each experiment the chosen linac settings voltage, charge and peak dose were recorded and tabulated in table 2. The conversion factor could not be confirmed in HIGS 2 and HIGS 3, so the pulse charge is unknown for the two experiments. The cathode was replaced between the HIGS 3 and HIGS 4 experiment leading to an updated conversion factor and accurate calculation of the pulse charge. In HIGS 6 the linac was tuned between two pulse charge settings on a given day leading to two different pulse charges. We can use the Faraday cup as a reference for dose but dosimetry is always done using EBT film.

Table 2: Tabulated are the voltage, conversion factor, charge, and peak dose of the HIGS FLASH pulse for a given experiment.

Experiment	Date	Voltage (V)	Conversion Factor (nC/V)	Charge (nC)	Peak Dose (Gy)
HIGS 1	April 6th, 2022	6.3	0.13	0.819	4
		1.7	0.13	0.221	1
		0.6	0.13	0.078	0.45
HIGS 2	May 4th, 2022	0.35	None	None	0.7
		0.7	None	None	1.5
		1.05	None	None	2.3
		1.2	None	None	2.4
HIGS 3	July 11th, 2022	1.6	None	None	4
HIGS 4	October 8th, 2022	2.4	0.85	2.04	5.4
HIGS 5	Nov 28th, 2022	0.45	0.85	0.38	1.03
HIGS 6a	January 10th, 2023	3	0.85	2.55	6.0
HIGS 6b	January 13th, 2023	2.3	0.85	1.96	4.4

The shape of the electron pulse supplied by the HIGS linac follows very closely to a 2D-gaussian distribution. The film techniques described earlier were implemented. The red color channel of film was imported into MATLAB, resized to 96 pixels per inch, gaussian smoothed with a standard deviation of 0.5 and the recorded dose to each pixel for a film was computed using film calibration curves. The resulting contour plot is shown in figure 9. This is a general representation of the normalized isodose lines except for HIGS 1, where a quadrupole magnet was used to shape the pulse into a more circular shape. In the shaping process a loss in pulse charge was noted. As the elliptical shape was large enough to cover the well and small enough to not spill into neighboring wells the quadrupole magnet was not used in later experiments.

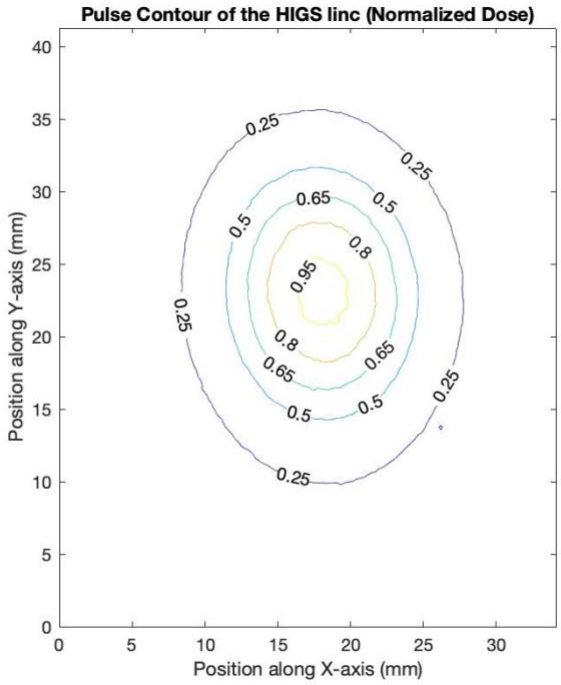

Figure 9: A typical dose map of the HIGS pulse. They demonstrate an elliptical shape well modeled by a 2D gaussian distribution.

The dose profile of one film measurement is shown in figure 10. Line profiles were taken through the major and minor axis of the elliptical pulse shape at the scan resolution of 400 DPI. The field size was determined by the FWHM of the line profiles and found to be around 1.3x2 cm^2. Both the major and minor axis of the ellipse are fitted with a gaussian curve. The sharp spike in the dose profile is a speck of dust on the film, an unfortunate artifact that may occasionally occur as scanning is done in an open-air environment. A Gaussian fit approximates the dose profile very nicely implying there is no overpowering low energy tail in the major axis direction and the energy spread is almost symmetrical around an energy of 34.439 MeV.

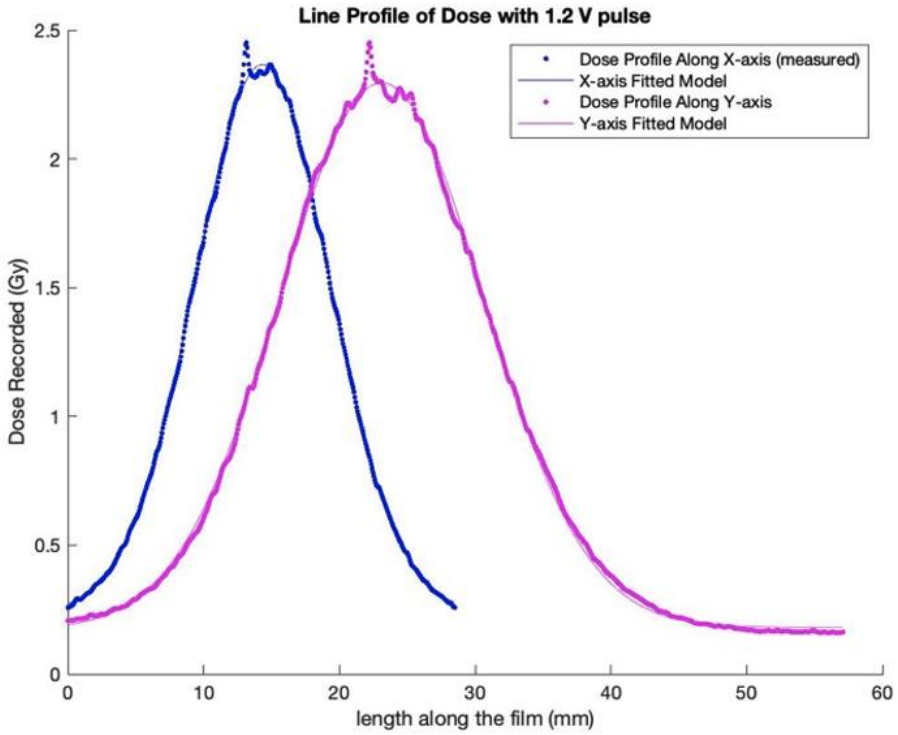

Figure 10: Dose profile of the HIGS pulse through the major and minor axis of the elliptical shape. Each dose profile was then fitted with a gaussian distribution.

A current transformer, placed just before the dipole, was used to find that the HIGS linac is capable of two pulse width settings of 100 ns and 1.2 μs. The repetition time achievable by the HIGS linac is 0.15 s. Following from this, 12 Gy can be delivered at a SSD of 18.4 cm with a MDR of 80 Gy/s. The IDR has been able to achieve as high as 40 MGy/s in HIGS 1 and anticipated to reach as high as 100 MGy/s.

2.2.2.2 Pulse Superposition and Targeting

One large question of the HIGS linac was its targeting capabilities. That is, will subsequent pulses strike the same point on film repeatably. To demonstrate the HIGS targeting capabilities, in the HIGS 4 experiment rows of wells were irradiated with 1 and

3 pulses, as seen in figure 12, each with a peak dose of 5.4 Gy at 18.4 cm SSD. Plates are held in a translational stage, closer to the exit window, and the dose per pulse was found to be 6.2 Gy ± 4%. Due to the high energy of the pulse and thin rat brain material it passes through we assume that dose to the slice and to the film is the same. The 3-pulse peak dose was found to be 18.4 Gy ± 4%. Given the gaussian nature of the pulse, this implies sufficient pulse repeatability and superposition to predict targeting and dose as the maxima of each pulse would need to align to achieve nearly 3x more dose than one pulse.

In addition, like figure 10, a line profile was taken through each well in both the major and minor axis. Comparison of the FWHM for 3 pulse and 1 pulse irradiation demonstrate the three pulse FWHM being 0.4 ± 0.2 mm smaller when compared to 1 pulse irradiations. We can claim that the pulse dose repeatability and targeting are within the sub-millimeter region and placement of the rat brain in the well is a larger source of error.

Table 3: HIGS 4 dosimetry data reporting the peak dose to each well for 5 plates. Three pulse peak dose is 3x greater than 1 pulse demonstrating superposition.

HIGS 4 Data Demonstrating Pulse Superposition											
Peak Dose to Well (Gy)		A1	A2	A3	A4	C1	C2	C3	C4	1 Pulse Avg	3 Pulse Avg
no 4T1	Film A	6.08	6.20	6.32	6.36	19.06	18.64	18.58	18.22	6.24	18.63
no 4T1	FIlm B	5.95	6.30	6.24	6.11	18.28	18.52	18.48	18.62	6.15	18.48
with 4T1	Film C	6.11	6.21	6.19	5.91	18.24	18.86	19.45	19.30	6.11	18.96
with 4T1	Film D	6.14	6.16	6.14	6.23	18.20	18.06	18.31	18.27	6.17	18.21
yH2AX	Film E	18.91	18.30	18.00	17.33	18.07	18.00	18.12	18.16		18.11
All Measurments are with 4% error										6.17	18.42

Targeting of a well was assured using a previously described method of irradiating all 4 corner wells and the two middle. By visual inspection the well walls are

discernable as electrons scatter out and attenuate through the 2 in thick plastic. In figure 11, each pulse is seen to be centered in the well and there is little to no dose spill over into a neighboring sample. Figure 11 was taken on site with an iPhone camera, some of the tunnel lighting can be seen reflecting in the film causing some artifacts.

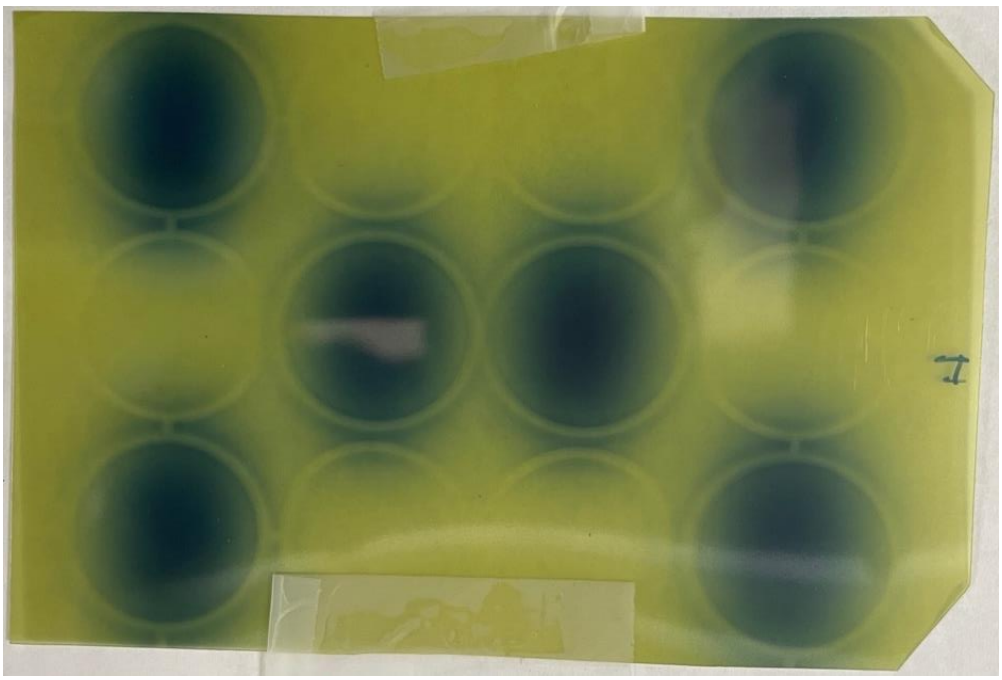

Figure 11: Final QA film pattern to demonstrate the good targeting of the translational stage.

Below, in figure 12, is another example of well targeting in which an image is captured mid irradiation and the scintillation light of the electrons passing through the plastic can be seen. A camera is placed above the exit window to observe, from the control room, the proper motion of the translational stage. Keeping in mind that the camera is tilted downward the electron pulse can be seen passing through the well and, more importantly, is contained inside the well.

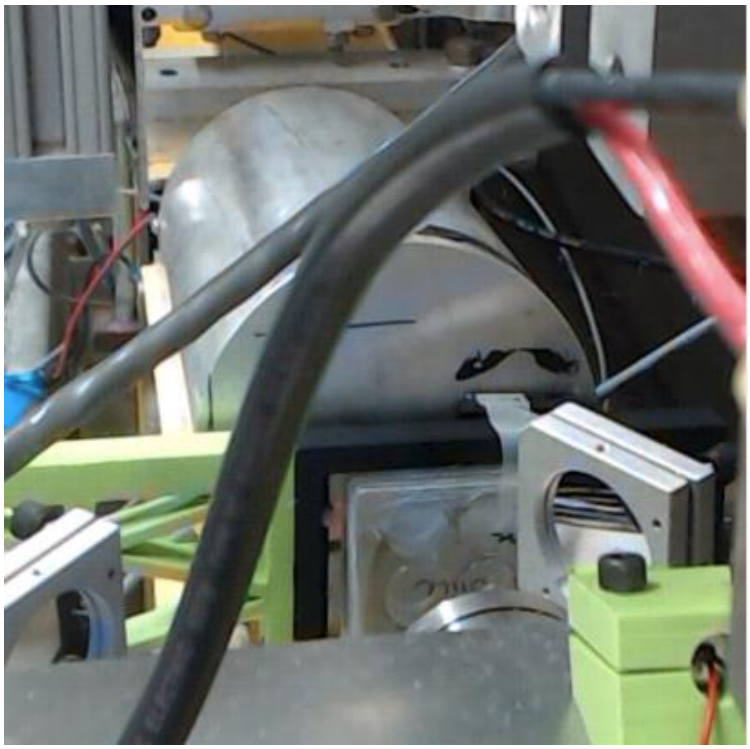

Figure 12: Mid-Irradiation image of the pulse passing through well C4.

2.2.2.3 Faraday Cup Model

In table 2 the voltage corresponding with a given peak pulse dose was noted. This voltage is proportional to the charge of each pulse and as the field size does not have a strong dependence on pulse charge, dose should also increase proportionally. In HIGS 2 the pulse charge was altered by heating the cathode of the electron gun allowing for variable dose from a pulse. The voltage measured using the Faraday cup plotted against the film measured peak dose can be used to examine both the linear relation of voltage to dose and the film being energy dependent for 20-35 MeV. Fitting of data shown in figure 13, allows us to predict pulse charge for a given Faraday cup voltage. The last data point suffers from not allowing enough time for the cathode heat up. This

allows for tunning the linac to a select voltage and have a predetermined dose for an experiment. In addition, a linear relation of the data implies that the calibration curve is still valid for this energy range as we would expect non-linear features to become apparent as we fitted the film calibration curve with a 3rd degree polynomial.

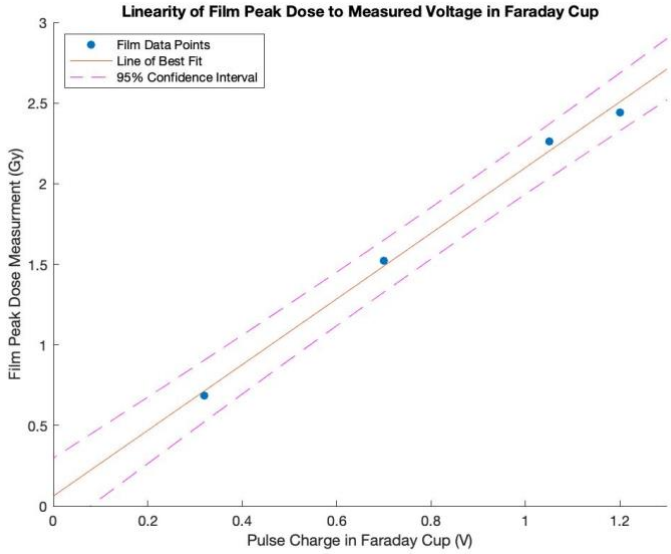

Figure 13: Pulse charge is recorded as a voltage in the faraday cup and can be plotted in relation to film measures dose per pulse.

Later experiments kept the pulse charge constant in the experiment, and it was found that the HIGS 2 Faraday cup model was incorrect by as much as 20%. To account for variability in the linac tuning a parameter file for a predetermined linac pulse was made and a Faraday cup model was made for the parameter file. Utilizing the dose superposition properties of the electron pulse we can irradiate with a varying number of pulses, record their voltages, and determine a linear relation between peak dose to sum of pulse voltages. This was performed in HIGS 4 and led to the following model:

$$D = 2.2580 \times V - 0.0527 \qquad (2.2)$$

Where D is the peak dose of the pulse, and V is the measured voltage on the Faraday cup. This model was used to successfully tune the linac to 1 Gy peak dose per pulse in HIGS 5a and HIGS 5b to within 3% of the target 1 Gy peak dose per pulse.

2.2.3 Discussion

The HIGS linac can achieve impressive IDR in the range of 1-100 MGy/s while maintaining a MDR greater than 40 Gy/s. This makes it one of the highest IDR machines currently being used for electron FLASH research (see figure 14 for comparison with other relevant linacs). This will allow the HIGS to explore a range of dose rate parameters and determine how tuning the dose rate can contribute to optimizing the FLASH-RT normal tissue sparing response.

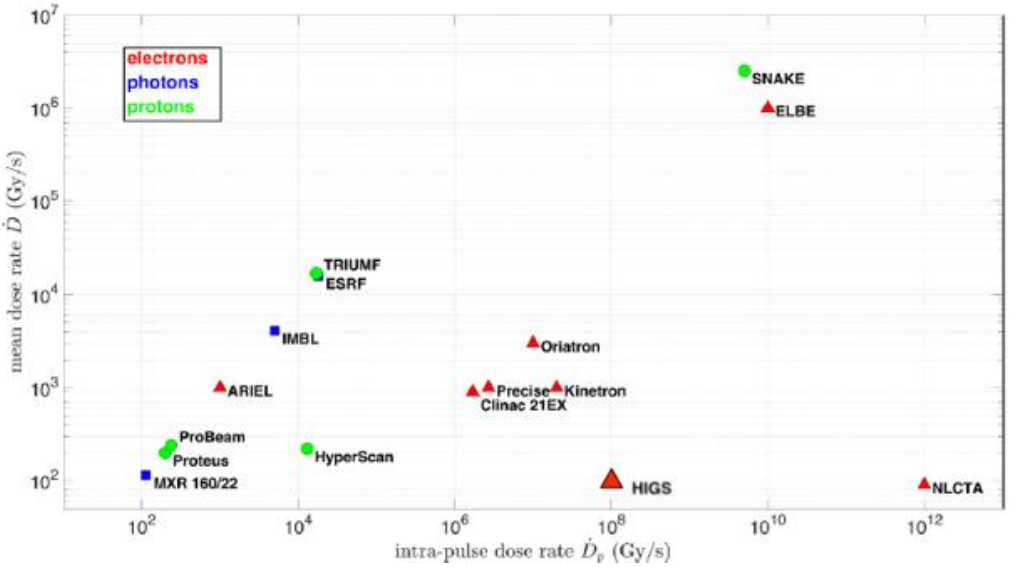

Figure 14: Comparison of the HIGS linac with other FLASH systems. Figure is adapted from Esplen et al. [16]

The remarkable repeatability and targeting capabilities of the HIGS linac allows for peace of mind in targeting a well. Well targeting errors to date have been due to human mistake rather than issues with the translational stage. Due to the near perfect targeting, dose can be easily escalated by increasing the number of pulses without fear of large alterations to the dose distribution and field size.

The Faraday cup model provides a reasonable way to tune the linac pulse charge to deliver a prescribed dose to each well and the pulse shape is suitable to cover the whole brain slice placed in the well. With each parameter file a new model is needed to approximate the shifts in pulse charge energy. With a known dose profile and a selected dose per pulse, treatment planning can be implemented to design experiments looking at specific doses as in HIGS 5, covered in Chapter 3.

2.3 Organotypic model imaging and segmentation

2.3.1 YFP Bleed Through Into mCherry Images

An organotypic rat brain model, seeded with 4T1 cancer cells, is used to observe normal tissue effects and to determine the cancer control of FLASH-RT in comparison with conventional irradiation methods. An issue presented itself wherein YFP signal from biolistically transfected normal neurons in the brain slice, imaged with the Enhanced Green Fluorescent Protein Filter (GFP), was presenting in the Rhodamine (Rhoda) filter used to image mCherry signal from 4T1 cells as seen in figure 15. The contrast is enhanced to see the neurons and 4T1 cells more clearly. The bright signal seen

in the left image corresponds to transfected neurons. Looking at the right image, one can see the same intense regions in the Rhoda filter from the YFP signal. This is known YFP signal as this effect is seen on slices without any cancer cells. The true mCherry signal is swamped and faintly visible in the center of the slice with weblike projections. The origin of YFP bleed-through signal is confirmed as being from healthy transfected neurons, as they will have a single bright axon stemming from them.

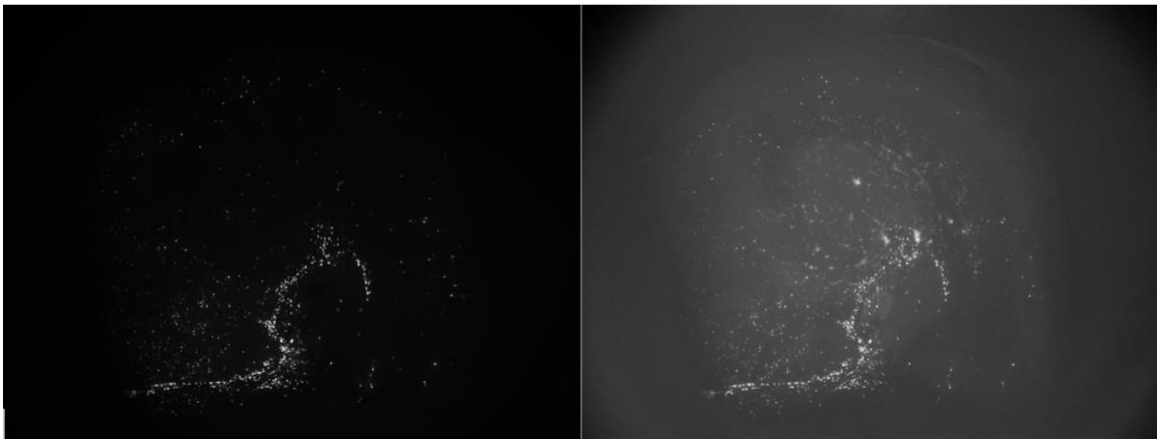

Figure 15: Left image is GFP filter only and right is Rhodamine filter. High intensity regions in both images are YFP signal bleeding through.

The bleeding through YFP signal of the healthy neurons can lead to a swamping of mCherry signal and prevent proper 4T1 segmentation. 4T1 segmentation is performed in CellProfiler [31] and the integrated intensity is used to be proportional to the number of 4T1 cells as demonstrated in previous work [29, 30]. Due to the worse signal to noise ratio, seen with visible inspection in figure 15, it is not possible, without some image enhancements, to determine a significant difference between different treatment arms.

2.3.2 Method of Bleed Through Removal and Segmentation

The process of YFP bleed through removal takes advantage of little to no movement in the well plate and microscope lens position between imaging with different filters. We can use the GFP image to determine pixels influenced by YFP signal needing to be overwritten or suppressed in the CellProfiler segmentation. Both GFP and Rhoda images were imported into MATLAB and a threshold was applied to the GFP image selecting high intense pixels to produce a mask of the YFP signal. This process was done manually, and no firm cutoffs exist. As the experiment progresses, from day 0 to day 5, the rat brain slice tends to become brighter. This results in manually increasing the threshold of selected intensity from day to day. The mask was then applied to the Rhoda image and pixels under the mask were replaced with a pixel value representative of the background. This was done by determining a starting background value at the center and then decreasing the overwritten pixel value following a decreasing linear function radially outward from the center of each image.

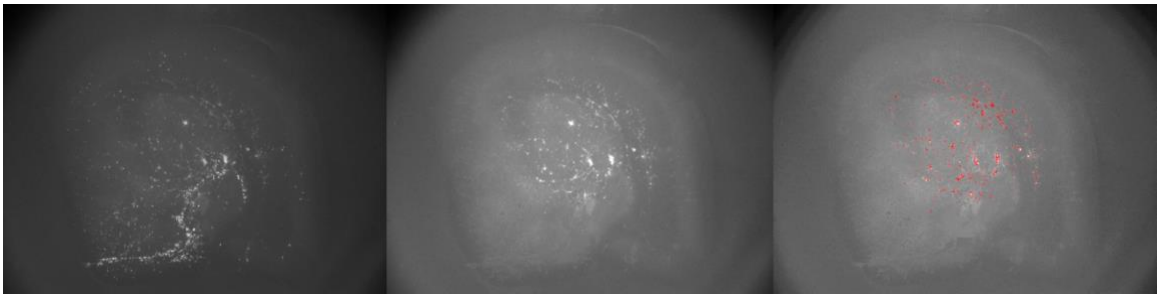

Figure 16: Left to Right: progression of raw image to image with removed YFP signal and lastly a properly segmented mCherry image.

The Rhoda image with removed YFP signal was then fed to CellProfiler and the pipeline parameters were tuned to select as much of the mCherry signal while omitting erroneous signal. These pipelines were kept the same across all images for a day but was slightly modified form day to day to account for the slow increase in background brightness and growing 4T1 colonies. The above figure 16 demonstrates the workflow of removing YFP signal from the Rhoda filter image and the resulting segmentation. When comparing the center to left image, the removal of YFP signal enhances the distinguishability of different 4T1 colonies. The resulting segmentation in CellProfiler results in a smooth segmentation with little noise and almost correctly segments all 4T1 colonies. In Chapter 3 we demonstrate that the results from this workflow are mirrored in an independent firefly luciferase assay (fFluc).

2.3.3 Results of Image segmentation with or without YFP signal

Signal removal of YFP from the rhodamine filter images of mCherry resulted in a set of YFP suppressed images. Following segmentation, the contoured mCherry signal intensity was integrated for a given well and averaged across all wells. The YFP suppression process was performed over all 4 days and then compared to data in which no YFP suppression was performed.

When segmenting the raw images in CellProfiler it was noted that a lot of background YFP signal is included in the final integration. Looking at the left plot in figure 17, no significant difference can be seen between the dark and the irradiated

plates. The signal from the unirradiated plate is only larger by a factor of about 1.5 than the signal from irradiated plates. There is even the suggestion that increasing dose beyond 6 Gy had a weaker effect in arresting 4T1 cell proliferation.

In the right plot of figure 17 we see the effects of YFP suppression, performed equally on unirradiated and irradiated plates. There is a clear separation between the unirradiated plate and both irradiated plates. The difference in integrated intensity between unirradiated and irradiated plates is by about a factor of 2. The YFP suppressed images suggest that 4T1 cell growth has ceased up to day 4 upon irradiation with 6 Gy or more. The final day also suggests the possibility that 4T1 cells in wells receiving 6 Gy begin to proliferate again; however, stronger statistics are needed to make this determination.

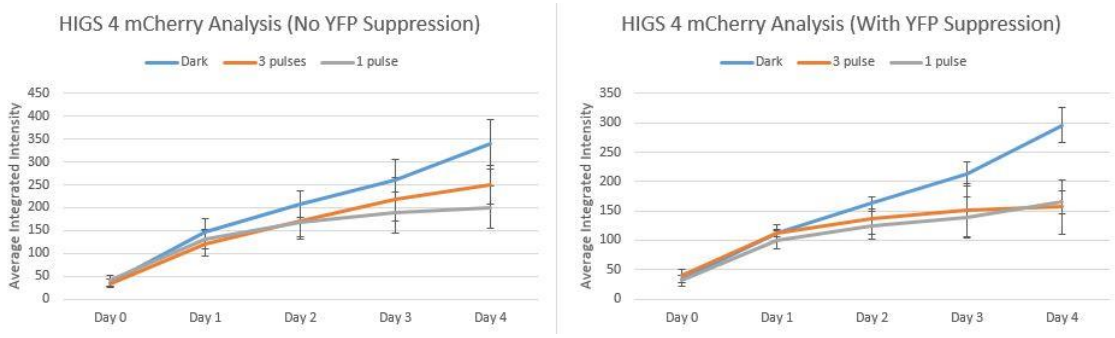

Figure 17: Comparison of YFP bleed through suppression techniques (right) with the original pipeline (left) from Russel et al. [30]

2.3.4 Discussion

YFP signal bleeding through the Rhoda filter swamps the true mCherry signal and hides the true biological response occurring in the 4T1 cancer cells. Using the

described YFP suppression techniques significantly increases performance of the CellProfiler segmentation pipeline and a sharp decline in the signal to noise can be observed. This improvement is clearly visible in the HIGS 4 mCherry analysis with and without the YFP bleed through.

The current method of determining the background signal, using a linear decreasing function emanating radially from the image center, works; however, it does not model the true additions to the background. Initially, the YFP suppression was intended as a temporary solution and future experiments would move to using Cyan FP or Green FP to prevent any bleed through. There has been some qualitative evidence that YFP can be used as a metric to measure normal tissue health, and due to its stronger signal compared to GFP and CFP it is preferred for an analysis of normal tissue. The next step would be to change the background function to model the true physics better. The functions to better model the slice and lighting background have been looked at before [29].

3. Final FLASH and Conventional Experiment Comparison

The techniques and procedures described in chapter 2 were incorporated into HIGS 5. The goal of experiment 5 was to take everything learned from the previous 4 HIGS FLASH experiments and create a final experiment to measure the cyto-toxic response of 4T1 cells to FLASH radiation dose rates using the HIGS compared to conventional irradiation. The secondary goal was to make a measurement of the normal tissue. Normal tissue observations are only a qualitative measure. There is also a γH2AX assay performed in HIGS 5, whose dosimetry data is included, but DNA damage results are not included in this thesis.

3.1 Methods and Approach of Experiment

3.1.1 Methods of HIGS 5

Rat brain slices were cut into 350 μm thick slices, shot with YFP, and placed on agarose in individual wells. 5 plates, with 8 slices across row A and C in each well of the plate, were prepared and seeded with 4000 mCherry fFluc 4T1 cells. The age of the rats used was 9 days postnatal. An example plate is shown earlier in figure 4. These comprised 4 treatment arms: 2 plates unirradiated, 1 plate irradiated with 2 pulses, one plate irradiated with 4 pulses, and a final plate irradiated with 6 pulses.

The HIGS linac was tuned to 0.45 V on the Faraday cup to achieve 1 ± 0.04 Gy per pulse on the beam dump. This voltage is determined using equation 2.2. The plate is

mounted on a 2D stage, calibrated with EBT-XD film to establish targeting positions, at a 9-degree incline to the beam direction. Discussed in section 4.2, dose shares an inverse relation with distance from the beam dump. The dose difference between row A and row C is expected to be 6% and can be checked with film dosimetry. The stage set up can be seen in figure 18.

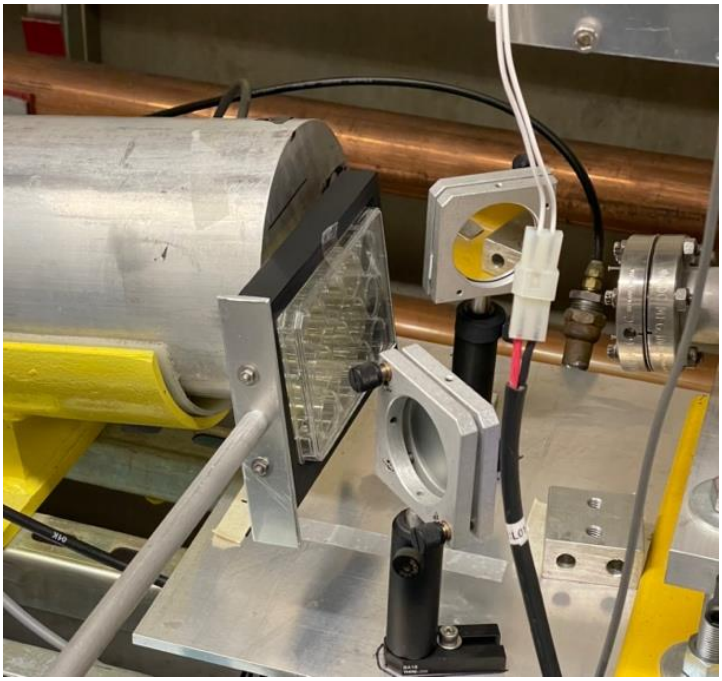

Figure 18: Image of well plate set up in HIGS 5 experiment. A 2D translational stage holds the plate at approximately 15 cm distance from the exit window.

The pulse width was conservatively placed at 100 ns resulting in a peak IDR of 1 MGy/s at an SSD of 18.4 cm. The repetition time per pulse was set to 0.4 s resulting in a MDR of 2.5 Gy/s. In HIGS 6 a MDR of greater than 40 Gy/s was achieved, but as one of our interests is the impact of IDR or MDR on FLASH-RT the dose rates of HIGS 5 satisfy a potential FLASH regime while maintaining pulse repeatability. As the plate sits closer

to the exit window than the beam dump, the true dose rates to each well are higher than predicted and dependent on which row the well is.

After irradiation, plates were imaged on a Zeiss stereoscope using an enhanced GFP and rhodamine filter to image the YFP and mCherry respectively. Dark plates were stood upright for 15 minutes to mimic treatment conditions. Imaging was done each day, with date of irradiation as day 0, and the time was recorded out to day 5. Following the last fluorescent image, an independent firefly luciferase readout was performed for comparison with the mCherry analysis. The mCherry analysis segmentation was performed as mentioned in chapter 3.

3.2.1 Methods of CONV 5

The CONV 5 experiment was designed to mirror the above experiment and contained 5 plates with the same organotypic model, type, and number of cancer cells. The age of the rats used in CONV 5 were 11 days postnatal. The treatment arms were also the same with 2 plates not being irradiated, 1 plate received 2.53 Gy, another 5.06 Gy and the final plate received 7.36 Gy. The prescribed doses are determined from film dosimetry of HIGS 5. Both mCherry and fFluc analysis were performed for comparison.

Irradiation was done with the Duke Radiation Oncology "Tan" machine, a Varian Clinac 21EX, set to 20 MeV electron mode with a dose rate of 1000 MU/min. Care was taken to account for the output factor of the cone and the PDD of 20 MeV electrons in dose calculations. To use the linac data tables and perform dose calculations, the plate

was placed on 9 cm of solid water for backscatter and the brain slice position was adjusted to 100 cm SSD. The green horizontal laser in figure 19 demonstrates how the linac couch was positioned to ensure that the brain slices reside at 100 SSD. Dose was assumed to be uniform to allow for irradiation of an entire plate with a single field. Given the gaussian dose profile used for FLASH irradiations, the small variability in non-uniformity of the conventional electron field is negligible.

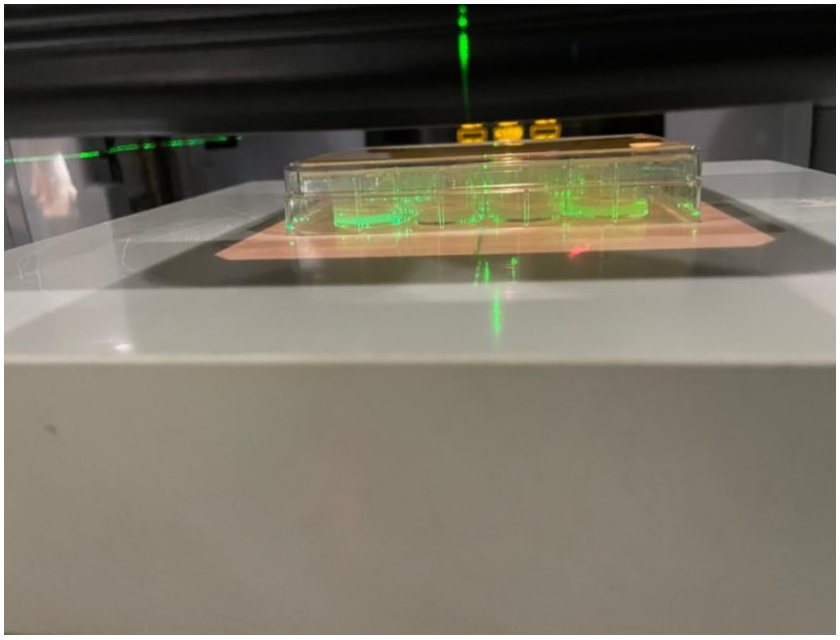

Figure 19: CONV 5 experiment set up on a Varian 2100 EX Clinac. SSD is set to put brain slice at 100 SSD.

After irradiation plates followed the same imaging procedure as in HIGS 5 except plates were not stood upright. Following the YFP and mCherry imaging to day 5 a fFluc readout was also performed for comparison. Both a mCherry and fFluc analysis were performed for comparison.

3.2 Results of Experiment HIGS 5 and CONV 5

As CONV was uniformly irradiated under a cone of a well calibrated medical linac, targeting and dose was not a major concern. For HIGS 5, EBT-XD film was attached to the back of the well plate and inserted into the holder. An image of film C, taped to the back of one of the plates, is shown in figure 20. It is cropped from the red color channel shown in gray scale of the original scanned image. Darker regions are high dose, and the position of each pulse can be related to the well walls seen as rings void of dose.

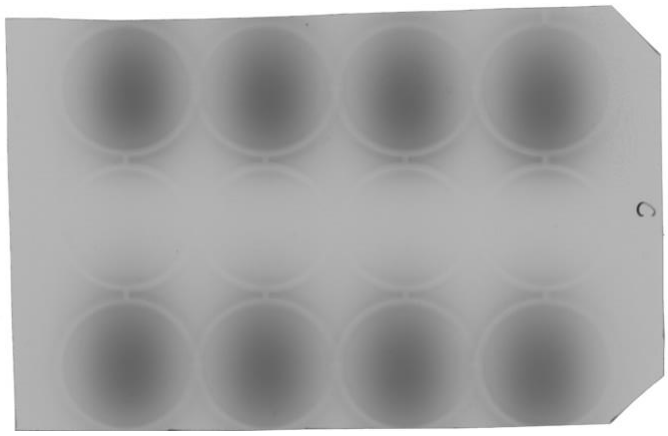

Figure 20: Demonstration of HIGS targeting. Pulse position can be inspected in relation to the well walls.

Dose was measured from the film, each irradiated as seen in figure 20, and knowing the center of row A is 2 inches above the center of row C we expect a 6% change in dose with the setup geometry when assuming an inverse fall off of dose. Table 4 tabulates the dose for all wells in HIGS 5 and records a ratio of average doses for Row A to Row C in each plate. The ratio of 0.94 demonstrated the predicted dose change of

6% and supports our understanding of the dose fall off for the HIGS linac. The peak dose to each well is reported in table 4 and has an error of 4% associated with each well's peak dose.

Table 4: Tabulated dose to each well in the HIGS 5 experiment. The dose per pulse at the brain slice was 1.2 Gy.

Dose (Gy)	A1	A2	A3	A4	C1	C2	C3	C4	A Row Average	C Row Average	Ratio
Plate 1	2.29	2.38	2.50	2.61	2.54	2.62	2.68	2.58	2.44	2.61	0.94
Plate 2	4.74	4.97	4.97	4.87	5.32	5.27	5.31	5.01	4.89	5.23	0.93
Plate 3	7.12	7.09	7.30	7.22	7.41	7.61	7.54	7.58	7.19	7.53	0.95
Plate 4 γH2AX	7.33	7.18	7.34	7.16	7.83	7.61	7.71	7.78	7.25	7.73	0.94

The mCherry and fFluc analysis are shown in figures 21 and 22. In figure 21 the 4T1 cancer cells in HIGS 5 underwent a plateau in their proliferation curve with increasing dose. This is equally reflected in the firefly luciferase reporter assay. The normal growth of 4T1 cancer cells begins to take place at later times as dose increases with plate receiving 7.36 Gy per well taking the longest to return to normal growth. The dark plates can be fitted with an exponential growth model with a doubling time of approximately 23 hours which is representative of the known doubling time of 4T1 cells.

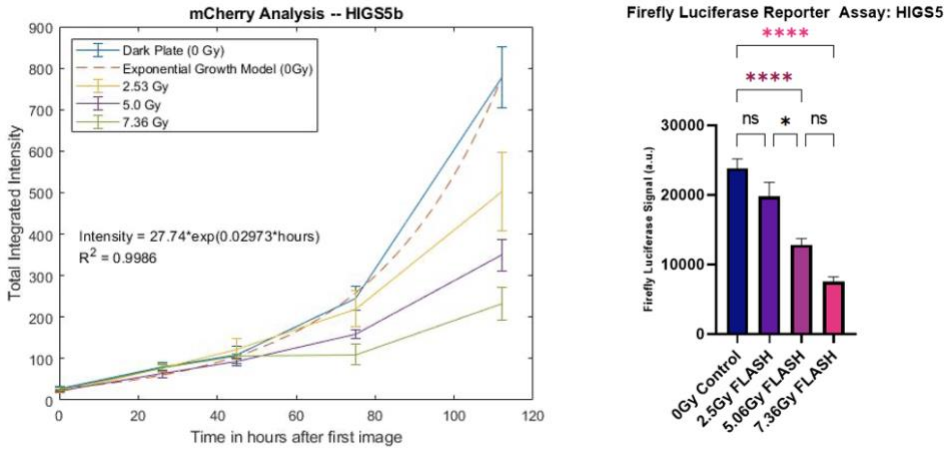

Figure 21: Left: mCherry CellProfiler analysis for HIGS 5. Right: Secondary fFluc analysis reflecting the findings of the mCherry Analysis.

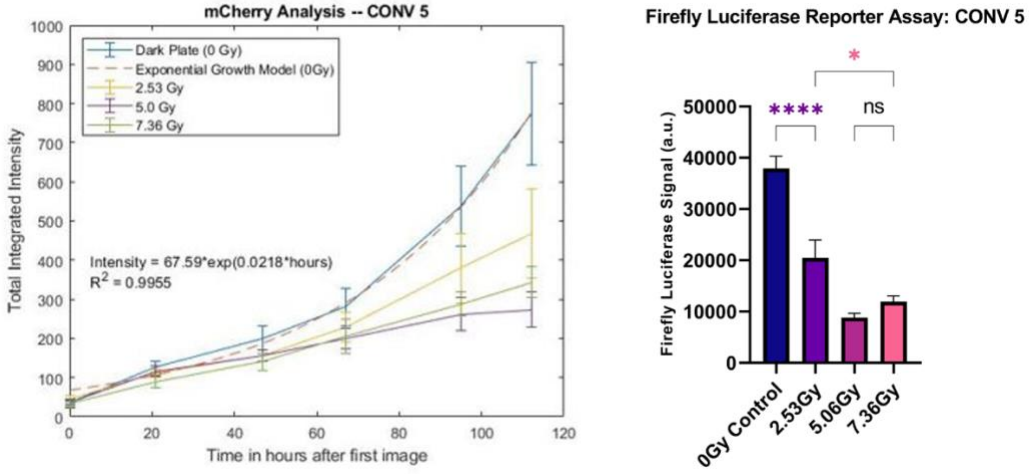

Figure 22: Left: mCherry CellProfiler Analysis for CONV 5. Right: Secondary fFluc analysis reflecting the findings of the mCherry Analysis.

In comparison, figure 22 shows a response of 4T1 proliferation to dose. There is an agreement between both the mCherry and fFluc reporter assay. Interestingly, the plate receiving 5.06 Gy seems to have had a larger cyto-toxic effect than 7.36 Gy. The

estimated doubling time of unirradiated cells from the exponential fit was 32 hours, about 10 hours longer than expected.

3.3 Discussion

The HIGS 5 experiment displayed the effectiveness of current film dosimetry techniques, our understanding of the HIGS beamline, targeting capabilities, and the ability to remove YFP bleed through from the mCherry image. Agreement between the mCherry and fFluc readout suggests that mCherry can be successfully used to image cells on a day-to-day basis and create a temporal map of their growth and the fFluc readout can confirm the final day results. A combination of the two measurements can be explored to further increase the sensitivity of the rat brain model at higher doses or tighter dose differences.

YFP bleed through removal in the CONV 5 experiment proved difficult. This may be indicative of the slice health compared to FLASH irradiation or it may be due to the difference in rat age between the two experiments. The brain slice will become brighter in later days and the background pixel intensities of CONV 5 were greater than 3,000 compared to 2,400 of HIGS 5. The difficulty in removing YFP signal leads to increased noise in the segmented mCherry image thus the SNR is not as strong. This explains certain features seen in figure 22 as there is no significant difference between the irradiated plates in the mCherry analysis and the second data point has a significant uptick in signal (YFP expression occurs 1 day after being transfected). The systematic

bias of YFP bleed through signal would also account for the increased doubling time of the unirradiated 4T1 cells. As YFP signal should not double in strength beyond one day post irradiation, bleed through of YFP would bias the data to show an increase in doubling time.

4. TOPAS Monte Carlo Simulation of the HIGS pulse

Dose modeling of the HIGS linac after beam extraction was explored with Monte Carlo Simulations using TOPAS. The motivation behind this was to create a tool to simulate dose distributions, explore linac characteristics and plan future experiments. A Monte Carlo simulation, accurately representing the HIGS linac, would also permit for dose planning for in vivo experiments using small animals.

4.1 Methods of Modeling the HIGS pulse

These simulations were constructed in TOPAS due to its ease in creating simulations and its potential to be expanded with TOPAS n' Bio to allow for modeling DNA damage [22, 23, 35]. HIGS presented a challenge in modeling as the electron pulse is extracted from the linac with a dipole at 9 degrees. As the energy spread of the pulse is not well known, modeling the beam divergence in the y-axis proved difficult. The energy spread in the pulse causes the electron pulse to diverge due to the magnetic field leading to the spread in the y-axis of the pulse and the elliptical dose shape. To approximate this effect, the vacuum beam line is made to be 2 meters long and the dipole effects to the beam divergence are approximated as a point source, 2 m from the aluminum exit window, with a divergence following a gaussian distribution. The assumes a gaussian spread of the electron energy around a mean value.

The major components of the model are the electron source, aluminum exit window, water film, and aluminum beam dump. The aluminum exit window is 0.03

inches thick with a diameter of 3 inches. The beam line before the exit window is a vacuum environment and air is placed between the exit window and beam dump. The water film is a 4x4 cm^2 slab of water with a thickness of 0.139 mm (the thickness of EBT3 and EBT-XD gafchromic film) [18, 19]. The water film is placed on the beam dump, which is modeled as a cylinder of aluminum with a length of 30 cm and a radius of 8 cm placed with an 18.4 cm gap of air between its face and the exit window. The set up can be seen in figure 23.

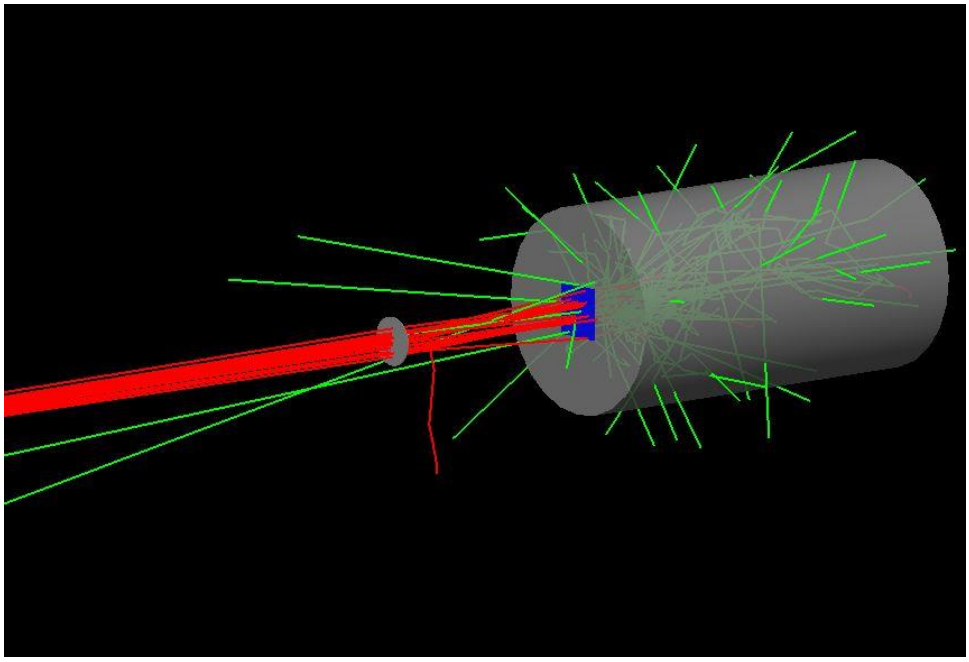

Figure 23: Monte Carlo set up of the HIGS electron beam. The electron beam (red tracks) dose is scored in the water film. Photon tracks are in green.

Dose scoring in the water film is performed with approximately 96 bins per inch, or a 151x151 matrix. The dose can be imported into MATLAB and compared with EBT-XD film measurements of the HIGS linac. Two simulations of interest to this paper were

run: one with 10^9 electrons and the water film placed on the beam dump to tune the electron divergence to match the dose map seen in EBT-XD film measurements and a second with 10^8 electrons where 3 films are placed at 18, 16 and 14 cm away from the exit window. The second simulation will allow for the comparison of HIGS linac simulated and measured dose fall off to an inverse fall off model.

4.2 Analysis between Simulated and Measured Dose maps

For the first film simulation, the simulated film was cropped to the same dimensions of an imported dose map from EBT-XD film measurements of HIGS 5 pulse and both dose maps were normalized. These were registered through minimizing the squared error between them and then compared through a gamma analysis. The two dose maps of the HIGS 5 simulated and measured pulse can be compared in figure 24 and look to agree nicely in appearance. EBT film was numbered with permanent marker, seen as a seven in the right plot of figure 24. These regions affected the gamma analysis as the criteria was set very tight. Both dose maps look to be very similar.

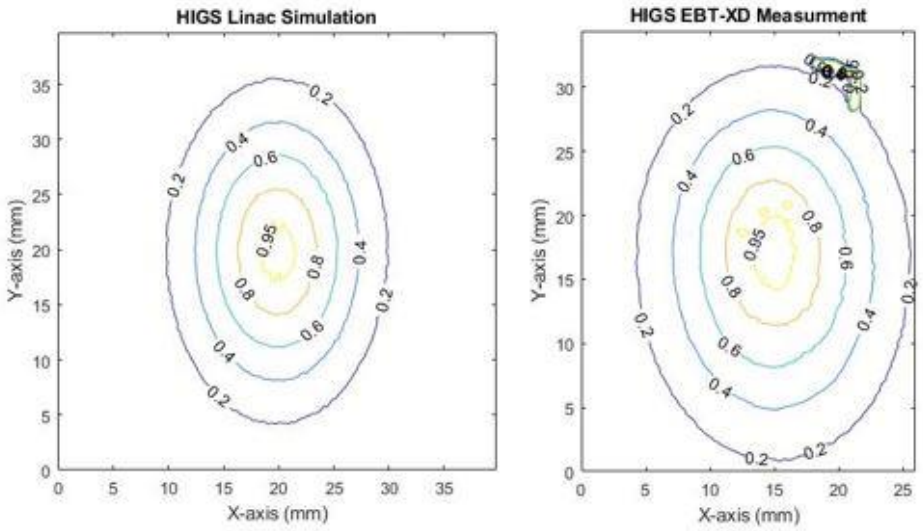

Figure 24: Left: TOPAS simulated dose profiles on a 4x4 cm² water film. Right: EBT-XD film dosimetry of the HIGS 5 pulse.

When performing a gamma analysis on the above figure, the criteria of 2%/2mm and a dose threshold of 10% was selected. This means a pixel on the simulated map was considered passing if a pixel on the measured was within 1 unit when normalizing the pixel distance and dose difference by 2mm and 2%. This analysis passed with a rate of 99.4% and only failing on the film edges or where dirt was on the film (such as marker). We can describe the gamma analysis as:

$$\gamma_n = min_m\left(\sqrt{\left(\frac{D_m - D_n}{\Delta D_t}\right)^2 + \left(\frac{d_m - d_n}{\Delta d}\right)^2}\right) \quad (3.1)$$

Where γ_n is a pixel of the measured dose map in comparison with all pixels, m, of the simulated dose map. The uppercase D is the dose for a pixel and the lowercase d is the position of the given pixel. The difference of dose or distance is normalized to

some threshold value in the denominator. The minimum distance value of all pixels is recorded. If γ is less than 1 then the pixel is considered passing, otherwise it fails.

The Registration and simulation quality can be further explored when looking at the dose profiles across the ellipses major and minor axis or x and y axis. These can be seen in figure 25. Both the simulated and measured dose profiles are in good agreement. There is some noise in the measured pulse which can make registration imprecise, and it seems the profile of the measured data is not perfectly symmetrical. Error bars are omitted on the plot but are within 4%. Interestingly, the line profiles do not perfectly match, possibly due to some tilting in the beam dump surface.

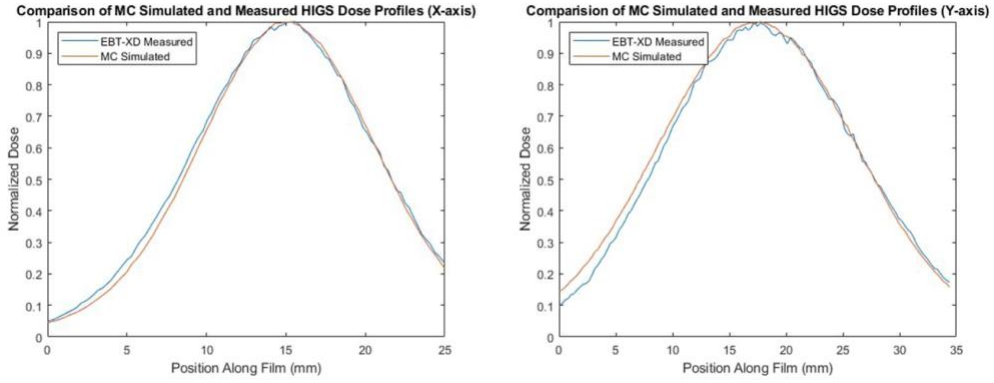

Figure 25: Comparison of Dose profiles between MC simulated and EBT-XD measured of both major axes.

The second simulation attempts to take a deeper look at the dose fall off. Film measurements note the HIGS linac dose decreasing with increasing distance from the exit window following an inverse relation. The peak dose to each of the three films was recorded and then normalized to dose at 14 cm distance from the exit window. Film measurements, from film attached to well plates across HIGS 1 to HIGS 5 and set at

specified distances, were normalized to the recorded dose at 14 cm and then overlayed onto the plot containing simulated values. Figure 26 compares simulate and measured results with an SSD of 18 cm. An inverse fall off model, normalized to 14 cm from the exit window, is plotted for comparison with simulations and measurements. The measured, simulated and inverse fall off model all look to agree reasonably well.

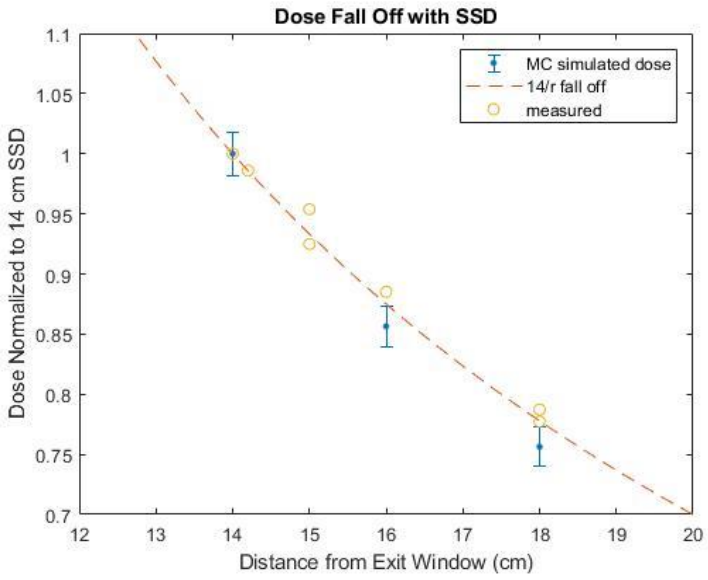

Figure 26: Dose fall off with increasing SSD from the exit window. (Normalized to 14 cm SSD)

4.3 Discussion

The HIGS Monte Carlo model, with a few assumptions, can recreate the dose map of the true EBT-XD film measured dose distribution. The differences in dose profiles could be due to rounding errors in the number of bins used to score the dose or even a slight tilt of the film when placed on the surface of the beam dump. Both could lead to small shifts in the dose profile, higher or lower. The simulation agrees with

measured data that the dose fall off in the 14-18 cm range follows an inverse fall off relation. This is most likely due to the high collimation of the pulse as it is striking the exit window. It is also not expected to be an inverse square relation as the electron field leaving the exit window is not truly a point source.

The modeling capabilities of this simulation are very close to what is observed in experiments. Iterative improvements can be made to the current simulation to increase its accuracy and better model linac components. Currently, the model is ready to be used to perform simple dose calculations for small animal irradiations when importing CT scans into TOPAS.

5. Conclusions

The High Intensity Gamma-ray Source is currently capable of impressive IDR dose rates reaching up to 100 MGy/s. As seen in figure 14, HIGS is among the highest IDR currently available. The tunable charge and adjustable pulse repetition time allows for traversing a broad range of IDR and MDR combinations and their effects to the FLASH effect. Coincidentally, the field size of the linac is approximately the size of a well and dose does not spill over into neighboring samples. The repeatability of a pulse in an experiment allows for precise and accurate targeting of wells and dose escalation with a series of pulses.

This thesis focuses on extracting the 35 MeV electron beam from the HIGS linac. There may be a benefit to further exploring the full capabilities of the HIGS facility. This includes the 180 MeV electron beam extraction point, 1.2 GeV electrons in the storage ring, and the resulting γ-ray beam. Each of these may provide unique discoveries, such as creating a larger FLASH photon field with the 180 or 35 MeV electron beam as performed by Gao et al. with a tungsten target [36]. Creating FLASH photon fields is currently a difficult task due to the heating of the tungsten target and in vivo studies are primarily performed with a synchrotrons [37]. Looking into methods of producing a reliable photon field that does not overly strain the tungsten target would be of great benefit to the FLASH-RT field and translating photon FLASH to clinical usage.

This work demonstrates the cytotoxic capabilities of the HIGS linac and how they are comparable to that of conventional irradiations. Though the CONV 5 results were not a perfect reflection of that seen in HIGS 5, they do provide a demonstration of the potential for observing the FLASH effect in less than 10 Gy. This was observed qualitatively by the tissue health generally being better for FLASH irradiation compared to conventional irradiation. It also lays the basis for future work to automate the YFP bleed through removal process and improve techniques developed here. In addition, the YFP signal can be further segmented for the potential of determining the radiation effects on normal tissue health.

Progress has been made in quantifying the cancer burden in the organotypic model. Even through there is some qualitative suggestions for tissue health, such as slice brightness under the stereoscope, further work can focus on quantifying the YFP signal and other signals, such as γH2AX, to look at DNA damage of the normal tissue. Some of this data has already been gathered and needs further analysis to determine if a method can be found to quantify the rat brain slice health.

The Monte Carlo simulations, constructed in TOPAS, are good models of the HIGS linac 2D dose profiles, and is representative of film measurements. Due to the HIGS being a widely used research accelerator for a variety of fields, the pulse architecture is consistently under alterations. Future work could look at automating the beam divergence tuning in the simulation to match the simulated dose profile to that of

the film measurements or a better model of the dipole effects could be simulated. Next steps would include a PDD of the 35 MeV HIGS electron beam and compare to simulations to further develop the model.

References

1. Vozenin, M.C., et al., *The Advantage of FLASH Radiotherapy Confirmed in Mini-pig and Cat-cancer Patients.* Clin Cancer Res, 2019. **25**(1): p. 35-42.

2. Montay-Gruel, P., et al., *Irradiation in a flash: Unique sparing of memory in mice after whole brain irradiation with dose rates above 100 Gy/s.* Radiotherapy and Oncology, 2017. **124**(3): p. 365-369.

3. Favaudon, V., et al., *Ultrahigh dose-rate FLASH irradiation increases the differential response between normal and tumor tissue in mice.* Science Translational Medicine, 2014. **6**(245).

4. Vozenin, M.C., J.H. Hendry, and C.L. Limoli, *Biological Benefits of Ultra-high Dose Rate FLASH Radiotherapy: Sleeping Beauty Awoken.* Clinical Oncology, 2019. **31**(7): p. 407-415.

5. Adrian, G., et al., *The FLASH effect depends on oxygen concentration.* British Journal of Radiology, 2020. **93**(1106).

6. Mascia, A.E., et al., *Proton FLASH Radiotherapy for the Treatment of Symptomatic Bone Metastases: The FAST-01 Nonrandomized Trial.* JAMA Oncol, 2023. **9**(1): p. 62-69.

7. Zhang, Y., et al., *Can Rational Combination of Ultra-high Dose Rate FLASH Radiotherapy with Immunotherapy Provide a Novel Approach to Cancer Treatment?* Clinical Oncology, 2021. **33**(11): p. 713-722.

8. Van Slyke, A.L., et al., *Oxygen Monitoring in Model Solutions and In Vivo in Mice During Proton Irradiation at Conventional and FLASH Dose Rates.* Radiat Res, 2022. **198**(2): p. 181-189.

9. Pratx, G. and D.S. Kapp, *Ultra-High-Dose-Rate FLASH Irradiation May Spare Hypoxic Stem Cell Niches in Normal Tissues.* International Journal of Radiation Oncology Biology Physics, 2019. **105**(1): p. 190-192.

10. El Khatib, M., et al., *Ultrafast Tracking of Oxygen Dynamics During Proton FLASH.* Int J Radiat Oncol Biol Phys, 2022. **113**(3): p. 624-634.

11. L. Newell, V.D., J. Clayton, et al., *In Regard to Rahman et al.* International Journal of Radiation Oncology Biology Physics, 2021. **110**(3): p. 908-909.

12. Rahman, M., et al., *Electron FLASH Delivery at Treatment Room Isocenter for Efficient Reversible Conversion of a Clinical LINAC.* International Journal of Radiation Oncology Biology Physics, 2021. **110**(3): p. 872-882.

13. *TUNL | Facilities, Free Electron Laser Laboratory and High Intensity Gamma-ray Source (HIGS)*. 2023 14, March 2023]; Available from: https://tunl.duke.edu/research/our-facilities.

14. Weller, H.R., et al., *Research opportunities at the upgraded HI gamma S facility.* Progress in Particle and Nuclear Physics, Vol 62, No 1, 2009. **62**(1): p. 257-303.

15. Small, K.L., et al., *Evaluating very high energy electron RBE from nanodosimetric pBR322 plasmid DNA damage.* Sci Rep, 2021. **11**(1): p. 3341.

16. Esplen, N., M.S. Mendonca, and M. Bazalova-Carter, *Physics and biology of ultrahigh dose-rate (FLASH) radiotherapy: a topical review.* Physics in Medicine and Biology, 2020. **65**(23).

17. Jorge, P.G., et al., *Dosimetric and preparation procedures for irradiating biological models with pulsed electron beam at ultra-high dose-rate.* Radiotherapy and Oncology, 2019. **139**: p. 34-39.

18. n.a. *Gafchromic Dosimetry Media, Type EBT-3*. Available from: http://www.gafchromic.com/documents/EBT3_Specifications.pdf.

19. n.a. *Gafchromic Dosimetry Media, Type EBT-XD*. Available from: http://www.gafchromic.com/documents/EBTXD_Specifications.pdf.

20. Lewis, D.F. and M.F. Chan, *Technical Note: On GAFChromic EBT-XD film and the lateral response artifact.* Medical Physics, 2016. **43**(2): p. 643-649.

21. Jaccard, M., et al., *High dose-per-pulse electron beam dosimetry: Usability and dose-rate independence of EBT3 Gafchromic films.* Med Phys, 2017. **44**(2): p. 725-735.

22. Faddegon, B., et al., *The TOPAS tool for particle simulation, a Monte Carlo simulation tool for physics, biology and clinical research.* Physica Medica-European Journal of Medical Physics, 2020. **72**: p. 114-121.

23. Perl, J., et al., *TOPAS: An innovative proton Monte Carlo platform for research and clinical applications.* Medical Physics, 2012. **39**(11): p. 6818-6837.

24. Sprenger, M., S. Brundage, and M. Oldham, *Modeling of Highly Spatially Fractionated Radiation Therapy (grid-RT) Through the Implementation of the Monte Carlo Software TOPAS for Optimization of Mini-GRID Design.* Medical Physics, 2022. **49**(6): p. E497-E497.

25. Rinkenbaugh, A.L., et al., *IKK/NF-kappa B signaling contributes to glioblastoma stem cell maintenance.* Oncotarget, 2016. **7**(43): p. 69173-69187.

26. Croft, C.L., et al., *Organotypic brain slice cultures to model neurodegenerative proteinopathies.* Molecular Neurodegeneration, 2019. **14**(1).

27. Daviaud, N., et al., *Organotypic cultures as tools for optimizing central nervous system cell therapies.* Experimental Neurology, 2013. **248**: p. 429-440.

28. Reinhart, P.H., et al., *Identification of anti-inflammatory targets for Huntington's disease using a brain slice-based screening assay.* Neurobiology of Disease, 2011. **43**(1): p. 248-256.

29. Holden, R., *An investigation of photo-activation of psoralen (AMT) during radiation therapy in a novel tissue model.* 2021, Duke University: Master's Thesis.

30. Holden, R., et al., *Evaluation of a method to measure fluorescent cell burden in complex culture systems.* Biomedical Physics & Engineering Express, 2022. **8**(3).

31. *CellProfiler | Free open-source software for quantitative analysis of biological images.* 2021; Available from: https://cellprofiler.org/.

32. Brundage, S., *Commissioning a State-of-Art Small Animal Irradiator and Novel Mini-GRID Treatment Technique*. 2022, Duke University: Master's Thesis.

33. Shameem, T., et al., *Effect of scanner lens on lateral response artefact in radiochromic film dosimetry.* Physical and Engineering Sciences in Medicine, 2022.

34. Lewis, D. and M.F. Chan, *Correcting lateral response artifacts from flatbed scanners for radiochromic film dosimetry.* Medical Physics, 2015. **42**(1): p. 416-429.

35. Schuemann, J., et al., *TOPAS-nBio: An Extension to the TOPAS Simulation Toolkit for Cellular and Sub-cellular Radiobiology.* Radiation Research, 2019. **191**(2): p. 125-138.

36. Gao, F., et al., *First demonstration of the FLASH effect with ultrahigh dose rate high-energy X-rays.* Radiother Oncol, 2022. **166**: p. 44-50.

37. Montay-Gruel, P., et al., *FLASH radiotherapy with photon beams.* Med Phys, 2022. **49**(3): p. 2055-2067.